Stepwise Oxidative C–C Coupling and/or C–N Fusion of Zn(II) meso -Pyridin-2-ylthio-porphyrins

Mathieu Berthelot, Fatima Akhssas, Abdou K D Dimé, Asmae Bousfiha, Julie Echaubard, Ghada Souissi, Hélène Cattey, Dominique Lucas, Paul Fleurat-Lessard, Charles H Devillers

Stepwise Oxidative C-C Coupling and/or C-N Fusion of Zn(II) *meso*-Pyridin-2-ylthio-Porphyrins

Mathieu Berthelot,[‡,[a]] Fatima Akhssas,[‡,[a]] Abdou K. D. Dimé,[[b]] Asmae Bousfiha,[[a]] Julie Echaubard,[[a]] Ghada Souissi,[[a]] Hélène Cattey,[[a]] Dominique Lucas,[[a]] Paul Fleurat-Lessard,[[a]] and Charles H. Devillers*[,[a]]

AUTHOR ADDRESS.

[a] Institut de Chimie Moléculaire de l'Université de Bourgogne, UMR6302, CNRS, Univ. Bourgogne Franche-Comté, 9 avenue Alain Savary, 21000 Dijon, France

[b] Département de Chimie, UFR SATIC, Université Alioune Diop de Bambey, Senegal

KEYWORDS. C-H Activation ; C-N Oxidative Fusion ; Electrosynthesis ; Porphyrinoids ; Pyridinium.

ABSTRACT. The synthesis and characterization of zinc(II) *meso*-pyridin-2-ylthio-porphyrins are presented in this manuscript. The (electro)chemical oxidation of [5-(pyridin-2-ylthio)-10,20-bis(*p*-tolyl)-15-phenylporphyrinato] zinc(II) or [5,15-bis(pyridin-2-ylthio)-10,20-bis(*p*-tolyl)porphyrinato] zinc(II) leads to the formation of one or two C-N bond(s) by intramolecular

nucleophilic attack of the peripheral thiopyridinyl fragment(s) on the neighboring β-pyrrolic position(s) (C-N fusion reaction). Besides, the chemical oxidation of [5-(pyridin-2-ylthio)-10,20-bis(*p*-tolyl)porphyrinato] zinc(II), *i.e.* bearing one free *meso* position, mainly affords the *meso*,*meso*-dimer. Further stepwise electrochemical oxidation selectively produces the mono and bis C-N fused *meso*,*meso*-dimer. The resulting pyridinium derivatives exhibits important changes in their physico-chemical properties (NMR, UV-vis., CV) as compared to their initial unfused precursors. Also the X-ray crystallographic structures of three unfused monomers, one unfused *meso*,*meso*-dimer and two C-N fused monomers are presented.

INTRODUCTION

Extending the π-conjugation of aromatic molecules *via* C-C or C-N coupling(s) with peripheral aromatic fragment(s) has been the focus of numerous researches over the last two decades.[1] As compared to their unfused precursors, the resulting extended structures demonstrate important modification of their electronic properties (bathochromic shift of their absorption/emission spectrum, two-photon cross-section increase, decrease of the HOMO-LUMO gap amongst others) and find applications in photovoltaic cells,[2,3] molecular electronics,[4] photodynamic therapy,[5] non-linear optical materials,[6] near-IR electroluminescence displays, just to mention a few.[7] More specifically with porphyrinoids, C-C and C-N fusion reactions have been performed starting with halogenated precursors,[8–10] using transition metals (silver,[11] iron,[12,13] copper, palladium,[9] scandium,[14] gold),[15] organic oxidants (DDQ, PIDA,[16] PIFA…), reducing agents such as $P(OEt_3)$,[17] by heating[18,19] or S_NAr reaction.[20] These syntheses are often performed under harsh conditions (oxidants in large excess, high temperature, acidic medium, etc.). When the π-system

is extended, the fused compounds are generally more easily oxidized that could lead to their oxidative overoxidation/degradation. In 2013 and 2014, Kadish, Gryko and co-workers presented the first examples of electrochemically-driven oxidative C-C fusion reaction between several porphyrin complexes (Zn(II), Ni(II), In(III), Ir(III)) and free-base with their peripheral dimethoxynaphtalene substituent.[21,22] In these reports, the authors showed that the formation of the porphyrin dication was required to promote the intramolecular C-C coupling. At the end of the electrolysis, the fused compounds were in their oxidized and reactive dicationic state. Thus to avoid their degradation, a consecutive reduction step was performed to recover their neutral state. Recently we speculated that a peripheral imine-based substituent would generate a positive charge during the oxidative intramolecular C-N coupling with the porphyrin core,[23] as already observed in an intermolecular fashion with pyridine.[24–32] Thus the fused compound may be more difficult to oxidize than its unfused precursor. Consequently, when applying a potential that corresponds to the first oxidation potential of the unfused precursor, the C-N fused target should not be overoxidized, contrarily to what can be often observed in common oxidative fusion process. Despite numerous examples of electrochemical C-N oxidative fusion in the literature,[33–37] only few examples described the preparation of C-N fused iminium derivatives. The first one was reported by Popp in 1972 and described the electrochemically-driven oxidative C-N fusion of a pyridinyl-naphthol derivative. After nucleophilic attack of the pyridine substituent on the oxidized naphthol fragment, a new 5-membered ring was formed and the pyridinium cation was obtained in low yield.[38] The second example was published in 2015 by the Yoshida's group.[39] In this report, an electrochemical intramolecular C-N coupling between the phenyl moiety and thio- or hydroxypyrimidine substituents was achieved in high yield affording new five-membered rings. It should be noted that the cyclized cationic products were not isolated and were used as

intermediates for the synthesis of pharmaceutical targets. In line with former studies that concerned peripheral reactivity of metalloporphyrins,[40–52] we reported in 2018 the oxidative C-N intramolecular coupling of nickel(II) *meso*-pyridin-2-ylthioporphyrins (**Ni-6**, **Ni-7** and **Ni-8**, M = Ni, Scheme 1).[23] The chemical and electrochemical oxidation of the porphyrins led to the formation of new cationic and planar fused compounds in good yields. As anticipated, the fused products were oxidized at higher potential than their unfused precursors that explained the good selectivity of the C-N fusion reaction. Moreover, a mechanism for the oxidative intramolecular C-N coupling reaction was proposed based on theoretical calculations and cyclic voltammetry analyses. It was shown that the porphyrin cation radical was very reactive ($t_{1/2} \leq 1$ ms range) and underwent a fast C-N fusion reaction. Besides, the fused compounds showed significant red bathochromic shift of their UV-visible absorption spectrum. In the continuity of this preliminary work on the C-N oxidative fusion of nickel(II) porphyrins, we present in this manuscript new developments with the zinc(II) complex analogues that demonstrate similar (for **Zn-6** and **Zn-8**, Scheme 1) but also totally different (for the *meso*-unsubstituted porphyrin **Zn-7**, Scheme 1) reactivities during their oxidation.

EXPERIMENTAL SECTION

Materials. Unless otherwise noted, all reactions were carried out without protection from air. CH_2Cl_2, MeCN and DMF were dried over alumina cartridges using a solvent purification system PureSolv PS-MD-5 model from Innovative Technology and kept under argon. All other solvents used for reactions were obtained from commercial suppliers and used as received. **1**, **2**, **Zn-2**, **3**, **4**, **5**, **Zn-5**, **6**, **7**, **8** were synthesized according to known procedures.[23,53–59] TLC were carried out on Merck DC Kieselgel 60 F-254 aluminium sheets. The spots were directly observed by naked eyes or through illumination with UV lamp (λ = 254/365 nm). Column chromatography

purifications were performed manually on silica gel (SiO_2, 40-63 µm, Sigma-Aldrich, technical grade).

Instruments and methods. ^{1}H-, ^{13}C-, ^{19}F- and ^{31}P-NMR spectra were recorded either on a Bruker Avance 300, on a Bruker Avance 500 or on a Bruker Avance 600 III HD spectrometer. Chemical shifts are expressed in parts per million (ppm) from the residual non-deuterated solvent signal.[60] *J* values are expressed in Hz. High-resolution mass spectra (HRMS) were recorded either on a Thermo LTQ Orbitrap XL apparatus equipped with an ESI source or on a Bruker UltraflexII LRF 2000 MALDI-TOF mass spectrometer (matrix: dithranol). UV-visible absorption spectra were recorded on a VARIAN Cary 50 UV-Visible spectrophotometer using quartz cells. Emission spectra were recorded on a JASCO FP8500 spectrofluorometer in a 10 mm path-length quartz cuvette (Starna) containing 1 mL of a solution of the zinc(II) complexes in DMSO. Measurement parameters were common for each measured compound: λ_{ex} = 447 nm, λ_{em} = 525-700 nm, Ex and Em slits = 5 nm, 1 nm pitch, 1 s response, scan speed = 200 nm·min^{-1}) at 20 °C.

Electrochemistry. All manipulations were performed using Schlenk techniques in an atmosphere of dry oxygen-free argon at room temperature (T = 20°C ± 3°C). The supporting electrolyte (tetraethylammonium tetrafluoroborate or tetra-*n*-butylammonium hexafluorophosphate ($TEABF_4$ or $TBAPF_6$) was degassed under vacuum before use and then dissolved in CH_2Cl_2 (unless otherwise noted) to a concentration of 0.1 mol L^{-1}. The following electrolyte volumes (unless otherwise noted) were used for voltammetric analyses and bulk electrolyses: anodic compartment: V = 20 mL; cathodic compartment: V = 5 mL; reference electrode compartment: V = 5 mL.

Cyclic Voltammetry. Voltammetric analyses were carried out in a standard three-electrode cell, with Biologic SP-300 potentiostat, connected to an interfaced computer that employed EC-Lab (v. 11.25) software. The reference electrode was a saturated calomel electrode (SCE) separated from the analyzed solution by a sintered glass disk filled with the background solution. The auxiliary electrode was a platinum foil separated from the analyzed solution by a sintered glass disk filled with the background solution. For all voltammetric measurements, the working electrode was a platinum electrode ($\varnothing$ = 2 mm). Before each voltammetric analysis, the Pt electrode was polished with a diamond suspension. In these conditions, when operating in CH_2Cl_2 (0.1 M $TBAPF_6$ or 0.1 M $TEABF_4$) or in CH_2Cl_2/CH_3CN 4:1 v/v (0.1 M $TEABF_4$), the formal potential for the ferrocene (+/0) couple was +0.46 V or +0.40 V *vs* SCE, respectively.

Bulk electrolyses. Bulk electrolyses were performed in CH_2Cl_2 0.1 M $TEABF_4$ (unless otherwise noted) at controlled potential in a cell with three compartments separated with glass frits of medium porosity with a Biologic SP-300 potentiostat, connected to an interfaced computer that employed EC-Lab (v. 11.25) software. Two platinum wire spirals (l = 50 cm, $\varnothing$ = 1 mm for each spiral, $S_{tot} \approx 2\times15 \approx 30$ cm^2) were used as working electrodes, a Pt plate (*ca*. 30 cm^2) or spiral (*ca.* 15 cm^2) was used as the counter electrode and a saturated calomel electrode was used as the reference electrode. Electrolyses were followed by TLC analyses and CV analyses and were stopped when the starting porphyrins were consumed.

Computational details

All DFT and TD-DFT calculations were performed using the Gaussian 16 package.[61] Energy and forces were computed by density functional theory with the hybrid B3PW91 exchange-correlation functional.[62] The solvent effects were modelled by means of the continuum model as implemented in Gaussian. In addition, dispersion effects have been considered using the D3

dispersion correction suggested by Grimme et al. with Becke-Johnson damping.[63] Geometries were optimized and characterized with the 6-31+G(d,p) basis set. Molecular orbitals were plotted using ChemCraft.[64] As the excited states are very delocalized (spanning over the full molecules), UV-visible simulations were conducted using the range-separated ωB97X-D functional[65] with the extended 6-311+G(2d,p) basis set.

Synthesis and characterization.

[5-(Pyridin-2-ylthio)-10,20-bis(*p*-tolyl)-15-phenylporphyrinato] zinc(II) Zn-6. A solution of 6[23] (187.15 mg, 2.78×10^{-1} mmol, 1.0 eq.) and $Zn(OAc)_2.2H_2O$ (121.61 mg, 5.54×10^{-1} mmol, 2.0 eq.) in $CHCl_3$ (17.5 mL) and CH_3OH (6.4 mL) was stirred at 60 °C for 1.5 h, monitoring the progress of the reaction by TLC (SiO_2, CH_2Cl_2). The solvent was then removed by rotary evaporation and the crude product was recrystallized in a CH_2Cl_2/CH_3OH mixture. The resulting precipitate was washed with CH_3OH and dried at 150 °C under vacuum for 1 h giving Zn-6 in 90% yield (184.14 mg, 2.49×10^{-1} mmol). ^{1}H NMR ($(CD_3)_2CO$ + one drop pyridine-d_5, 500 MHz, 298 K): δ (ppm) 9.87 (d, $^3J_{H\text{-}H}$ = 4.6 Hz, 2H), 8.92 (d, $^3J_{H\text{-}H}$ = 4.6 Hz, 2H), 8.84 (d, $^3J_{H\text{-}H}$ = 4.6 Hz, 2H), 8.83 (d, $^3J_{H\text{-}H}$ = 4.6 Hz, 2H), 8.34 (ddd,$^3J_{H\text{-}H}$ = 4.9 Hz, $^4J_{H\text{-}H}$ = 1.9 Hz, $^5J_{H\text{-}H}$ = 0.9 Hz, 1H), 8.21 – 8.18 (m, 2H), 8.07 (d, $^3J_{H\text{-}H}$ = 7.9 Hz, 4H), 7.83 – 7.74 (m, 3H), 7.59 (d, $^3J_{H\text{-}H}$ = 7.4 Hz, 4H), 7.00 (ddd, $^3J_{H\text{-}H}$ = 8.4 Hz, $^3J_{H\text{-}H}$ = 7.4 Hz, $^4J_{H\text{-}H}$ = 1.9 Hz, 1H), 6.87 (ddd, $^3J_{H\text{-}H}$ = 7.4 Hz, $^3J_{H\text{-}H}$ = 4.9 Hz, $^4J_{H\text{-}H}$ = 0.9 Hz, 1H), 5.91 (d, $^3J_{H\text{-}H}$ = 8.4 Hz, 1H), 2.68 (s, 6H); $^{13}C\{^1H\}$ NMR ($(CD_3)_2CO$ + one drop pyridine-d_5, 126 MHz, 298 K): δ (ppm) 155.8, 151.8, 151.7, 140.9, 138.0, 137.3, 135.2, 135.1, 134.0, 132.9, 132.4, 128.5, 128.0, 127.3, 122.5, 121.7, 119.9, 21.5; R_f 0.66 (SiO_2, CH_2Cl_2); λ_{max} (CH_2Cl_2) / nm (log ε): 424 (5.72), 552 (4.34), 591 (3.74); HRMS (ESI+): *m/z* cald for $C_{45}H_{32}N_5SZn$ $[M + H]^+$ 738.16644, found 738.16678.

[5-(Pyridin-2-ylthio)-10,20-bis(*p*-tolyl)porphyrinato] zinc(II) Zn-7. A solution of **7**[23] (403.01 mg, 6.72×10^{-1} mmol, 1.0 eq.) and $Zn(OAc)_2.2H_2O$ (294.97 mg, 1.34 mmol, 2.0 eq.) in $CHCl_3$ (42.5 mL) and CH_3OH (15.4 mL) was stirred at 60 °C for 1.5 h, monitoring the progress of the reaction by TLC (SiO_2, CH_2Cl_2). The solvent was then evaporated and the crude product was recrystallized in CH_2Cl_2/CH_3OH mixture. The precipitate obtained was washed with CH_3OH and dried at 110 °C overnight to give **Zn-7** in 89% yield (397.52 mg, 6.0×10^{-1} mmol). ^{1}H NMR ($(CD_3)_2SO$, 500 MHz, 298 K): δ (ppm) 10.40 (s, 1H), 9.82 (d, $^3J_{H\text{-}H}$ = 4.6 Hz, 2H), 9.48 (d, $^3J_{H\text{-}H}$ = 4.4 Hz, 2H), 8.89 (d, $^3J_{H\text{-}H}$ = 4,5 Hz, 4H), 8.38 (d, $^3J_{H\text{-}H}$ = 4,5 Hz, 1H), 8.08 (d, $^3J_{H\text{-}H}$ = 7.4 Hz, 4H), 7.61 (d, $^3J_{H\text{-}H}$ = 7,4 Hz, 4H), 7.17 (br dd, 1H), 6.95 (br dd, 1H), 6.07 (d, $^3J_{H\text{-}H}$ = 8.4 Hz, 1H), 2.68 (s, 6H); $^{13}C\{^1H\}$ NMR ($(CD_3)_2SO$, 126 MHz, 298 K): δ (ppm) 165.3, 153.6, 150.2, 149.9, 149.0, 148.9, 139.3, 137.0, 136.8, 134.2, 133.0, 132.7, 131.8, 131.5, 127.3, 120.9, 120.6, 119.4, 108.6, 103.1, 21.1; R_f 0.48 (SiO_2, CH_2Cl_2); λ_{max} (CH_2Cl_2) / nm (log ε): 306 (4.16), 419 (5.52), 547 (4.18); HRMS (ESI+): *m/z* cald for $C_{39}H_{28}N_5SZn$ $[M + H]^+$ 662.13514, found 662.13721.

Bis-*meso*,*meso*-linked-[5-(Pyridin-2-ylthio)-10,20-bis(*p*-tolyl)porphyrinato] zinc(II) (Zn-7)$_2$. A solution of **Zn-7** (841.35 mg, 1.269 mmol, 1.0 eq.), K_2CO_3 (353.56 mg, 2.558 mmol, 2.0 eq.) and PIFA (327.29 mg, 0.761 mmol, 0.6 eq.) in $CHCl_3$ (200 mL) was stirred at room temperature for 75 min. Then 1.5 mL of pyridine were added and the solvent was then evaporated. The crude product was purified by column chromatography (SiO_2, CH_2Cl_2/*n*-heptane/pyridine (70:29.5:0.5 v/v), *h* = 20 cm, *Ø* = 7.5 cm). After discarding the two first blue (unknown product) and pink/purple (**Zn-7**) fractions, the polarity of the eluent was increased (CH_2Cl_2/pyridine (99.5:0.5 v/v). The third yellow/green/brown fraction corresponded to **(Zn-7)$_2$**. This latter was recrystallized in a CH_2Cl_2/*n*-pentane mixture. The precipitate was washed with *n*-pentane and dried at 150 °C under vacuum for 3 h to give **(Zn-7)$_2$** in 71% yield (761.33 mg,

0.451 mmol, the molecular weight of **(Zn-7)$_2$** was calculated with 4.6 molecules of pyridine (*M.W.*= 1688.0932 g.mol^{-1}), in agreement with the ^{1}H NMR spectrum of **(Zn-7)$_2$** in DMSO, see Figure S18). ^{1}H NMR (THF-d_8, 500 MHz, 298 K): δ (ppm) 9.96 (d, $^3J_{H\text{-}H}$ = 4.7 Hz, 4H), 8.94 (d, $^3J_{H\text{-}H}$ = 4.7 Hz, 4H), 8.51 (d, $^3J_{H\text{-}H}$ = 4.6 Hz, 4H), 8.34 (d, $^3J_{H\text{-}H}$ = 4.5 Hz, 2H), 8.07 (d, $^3J_{H\text{-}H}$ = 8.0 Hz, 8H), 7.98 (d, $^3J_{H\text{-}H}$ = 4.6 Hz, 4H), 7.48 (d, $^3J_{H\text{-}H}$ = 8.0 Hz, 8H), 7.02 (m, 2H), ~6.83 (m, 2H), 6.13 (d, $^3J_{H\text{-}H}$ = 8.2 Hz, 2H), 2.59 (s, 12H); ^{13}C{^{1}H} NMR (THF-d_8, 126 MHz, 298 K): δ (ppm) 155.9, 155.3, 152.2, 151.2, 149.7, 148.8, 141.2, 137.8, 136.9, 136.7, 135.1, 134.6, 133.6, 132.5, 131.9, 127.8, 124.1, 123.2, 122.7, 121.9, 119.6, 105.9; 21.4; R_f 0.11 (SiO_2, CH_2Cl_2); λ_{max} (DMSO) / nm (log ε): 323 (4.61), 432 (5.44), 468 (5.51), 574 (4.78), 624 (4.34); HRMS (ESI+): *m/z* cald for $C_{78}H_{53}N_{10}S_2Zn_2$ $[M + H]^+$ 1321.24735, found 1321.24507.

[5,15-Bis(pyridin-2-ylthio)-10,20-bis(*p*-tolyl)porphyrinato] zinc(II) Zn-8. A solution of **8** (154.80 mg, 2.18×10^{-1} mmol, 1.0 eq.) and $Zn(OAc)_2.2H_2O$ (95.90 mg, 4.37×10^{-1} mmol, 2.0 eq.) in a mixture of $CHCl_3$ (13.8 mL) and CH_3OH (5.0 mL) was stirred at 60 °C for 1.5 h, monitoring the progress of the reaction by TLC (SiO_2, CH_2Cl_2). The solvent was then removed by rotary evaporation and the crude product was recrystallized in a CH_2Cl_2/CH_3OH mixture. The precipitate obtained was washed with CH_3OH and dried at 150 °C under vacuum for 1.75 h to give **Zn-8** in 93% yield (157.60 mg, 2.04×10^{-1} mmol). ^{1}H NMR ($(CD_3)_2SO$, 500 MHz, 298 K): δ (ppm) 9.80 (d, $^3J_{H\text{-}H}$ = 4.7 Hz, 4H), 8.82 (d, $^3J_{H\text{-}H}$ = 4.7 Hz, 4H), 8.35 (ddd, $^3J_{H\text{-}H}$ = 4.9 Hz, $^4J_{H\text{-}H}$ = 1.8 Hz, $^5J_{H\text{-}H}$ = 0.9 Hz, 2H), 8.05 (d, $^3J_{H\text{-}H}$ = 7.8 Hz, 4H), 7.60 (d, $^3J_{H\text{-}H}$ = 7.8 Hz, 4 H), 7.24 (ddd, $^3J_{H\text{-}H}$ = 8.4 Hz, $^4J_{H\text{-}H}$ = 7.4 Hz, $^4J_{H\text{-}H}$ = 1.8 Hz, 2H), 6.98 (ddd, $^3J_{H\text{-}H}$ = 7.3 Hz, $^4J_{H\text{-}H}$ = 4.9 Hz, $^5J_{H\text{-}H}$ = 0.9 Hz, 2H), 6.16 (d, $^3J_{H\text{-}H}$ = 8.4 Hz, 2H), 2.63 (s, 6H); R_f 0.11 (SiO_2, CH_2Cl_2); λ_{max} (CH_2Cl_2) / nm (log ε): 320 (4.34), 436 (5.65), 568 (4.11), 601 (3.96), 623 (4.12); HRMS (ESI+): *m/z* cald for $C_{44}H_{31}N_6S_2Zn$ $[M + H]^+$ 771.13376, found 771.13602.

Fused [5-(Pyridin-2-ylthio)-10,20-bis(*p*-tolyl)-15-phenylporphyrinato] zinc(II) (Zn-6$^+$,PF$_6^-$). ***Chemical oxidation.*** A solution of **Zn-6** (50.01 mg, 6.77×10^{-2} mmol, 1.0 eq.), PIFA (29.12 mg, 6.77×10^{-2} mmol, 1.0 eq.) and K_2CO_3 (18.97 mg, 1.36×10^{-1} mmol, 2.0 eq.) in dry CH_2Cl_2 (12.5 mL) was stirred at room temperature for 1 h, monitoring the progress of the reaction by TLC (SiO_2, CH_2Cl_2). At that time, an additional amount of PIFA (5.83 mg, 1.36×10^{-2} mmol, 0.2 eq.) was added. After 1 h, the solvent was evaporated. The crude product which bears the CF_3COO^- counter-anion, as attested by ^{19}F NMR analysis, was eluted with CH_3CN through an anion-exchange resin (AMBERLIT^{TM} IRA 96 resin) previously saturated with PF_6^- anions. The solvent was then removed under vacuum and the product was recrystallized in a CH_2Cl_2/*n*-hexane mixture. The precipitate was washed with *n*-hexane and dried at 150 °C under vacuum for 2.5 h giving **Zn-6$^+$,PF$_6^-$** in 91% yield (54.72 mg, 6.20×10^{-2} mmol). ***Electrochemical oxidation.*** **Zn-6** (50.05 mg, 6.77×10^{-2} mmol, 1.0 eq.) was electrolyzed at E_{app} = 0.86 V/SCE in 20 mL of CH_2Cl_2 0.1 M $TEABF_4$ containing pyridine (1 eq.) and K_2CO_3 (2 eq.) under Ar, at RT, under vigorous stirring. After abstraction of 2.0 ± 0.1 F/mol of porphyrin, the organic phase was washed three times (3×50 mL) with water to remove the supporting electrolyte. The organic solvent was evaporated and the crude mixture, which bears the BF_4^- counter-anion, as attested by ^{19}F NMR analysis, was eluted with CH_3CN through an anion exchange resin (AMBERLIT^{TM} IRA96 resin) previously saturated with PF_6^- anions. The solvent was then removed under vacuum. The product was recrystallized in a CH_2Cl_2/*n*-hexane mixture. The precipitate obtained was filtered under vacuum, washed with *n*-hexane and dried at 150 °C under vacuum for 5 h to give **Zn-6$^+$,PF$_6^-$** in 83% yield (49.56 mg, 5.61×10^{-2} mmol). ^1H NMR ($(CD_3)_2SO$, 500 MHz, 298 K): δ (ppm) 10.38 (d, $^3J_{H\text{-}H}$ = 6.6 Hz, 1H), 9.71 (s, 1H), 9.51 (d, $^3J_{H\text{-}H}$ = 4.6 Hz, 1H), 8.93 (d, $^3J_{H\text{-}H}$ = 4.7 Hz, 1H), 8.87 (d, $^3J_{H\text{-}H}$ = 4.6 Hz, 1H), 8.85 (d, $^3J_{H\text{-}H}$ = 4.6 Hz, 1H), 8.81 (d, $^3J_{H\text{-}H}$ = 4.7

Hz, 1H), 8.78 (d, $^{3}J_{H\text{-}H}$ = 4.6 Hz, 1H), 8.54 (d, $^{3}J_{H\text{-}H}$ = 4.1 Hz, 1H), 8.39-8.34 (m, 1H), 8.21-8.18 (m, 2H), 8.14 (d, $^{3}J_{H\text{-}H}$ = 7.7 Hz, 2H), 8.11 (d, $^{3}J_{H\text{-}H}$ = 7.7 Hz, 2H), 8.04-8.01 (m, 1H), 7.88-7.81 (m, 3H), 7.72 (d, $^{3}J_{H\text{-}H}$ = 7.5 Hz, 2H), 7.66 (d, $^{3}J_{H\text{-}H}$ = 7.6 Hz, 2H), 2.76 (s, 3H), 2.71 (s, 3H); $^{13}C\{^{1}H\}$ NMR ($(CD_3)_2SO$, 151 MHz, 298 K): δ (ppm) 151.3, 151.3, 150.8, 149.6, 148.9, 146.0, 142.6, 142.1, 138.6, 137.2, 134.3, 134.2, 134.1, 133.4, 128.0, 127.5, 126.8, 21.3, 21.1; ^{19}F NMR ($(CD_3)_2SO$, 470 MHz, 298 K): δ (ppm) -70.15 (d, $^{1}J_{F\text{-}P}$ = 712.0 Hz); ^{31}P NMR ($(CD_3)_2SO$, 202 MHz, 298 K): δ (ppm) -144.20 (hept, $^{1}J_{P\text{-}F}$ = 711.0 Hz); R_f 0.52 (SiO_2, CH_2Cl_2/CH_3OH (9:1, v/v)); λ_{max} (CH_2Cl_2) / nm (log ε): 320 (4.41), 432 (5.23), 573 (4.10), 613 (4,01); HRMS (ESI+): *m/z* cald for $C_{45}H_{30}N_5SZn$ $[M - PF_6]^+$ 736.15079, found 736.15159.

Fused [5,15-Bis(pyridin-2-ylthio)-10,20-bis(*p*-tolyl)porphyrinato] zinc(II) Zn-8$^+$,PF$_6^-$. ***Chemical oxidation.*** **Zn-8** (49.99 mg, 64.7 μmol, 1.0 eq.), K_2CO_3 (18.07 mg, 1.29×10^{-1}, 2.0 eq.) and PIFA (27.84 mg, 6.47×10^{-2} mmol, 1.0 eq.) were introduced in a dry round bottom flask. Dry CH_2Cl_2 (12.5 mL) was added and the mixture was stirred at room temperature for 1 hour, monitoring the progress of the reaction by TLC (SiO_2, CH_2Cl_2). At that time, an additional amount of PIFA (5.56 mg, 1.29×10^{-2} mmol, 0.2 eq.) was added. After 1 hour, the solvent was evaporated. The crude product which bears the CF_3COO^- counter-anion, as attested by ^{19}F NMR analysis, was eluted with CH_3CN through an anion-exchange resin (AMBERLIT^{TM} IRA96 resin) previously saturated with PF_6^- anions. The solvent was the removed under vacuum and the product was purified by column chromatography (SiO_2, CH_2Cl_2/CH_3OH (from 98:2 to 9:1, v/v) containing Et_3N (1%, v/v)). Two fractions were collected, containing traces of unreacted porphyrin **Zn-8** (Fraction 1) and **Zn-8$^+$,PF$_6^-$** (Fraction 2) and a third one was stucked on the top of the column. Fraction 2 was recrystallized in CH_2Cl_2/*n*-hexane. The precipitate was filtered under vacuum, washed with *n*-hexane and dried at 150 °C under vacuum for 1.5 h to give **Zn-**

8$^+$,PF$_6^-$ in 60 % yield (35.50 mg, 3.87×10^{-2} mmol). ***Electrochemical oxidation.*** **Zn-8** (50.01 mg, 64.8 µmol) was electrolyzed at E_{app} = 1.00 V/SCE in 20 mL of CH_2Cl_2 0.1 M $TEABF_4$ containing pyridine (1 eq.) and K_2CO_3 (2 eq.) under Ar, at RT, under vigorous stirring. After abstraction of 2.0 ± 0.1 F/mol of porphyrin, the organic phase was washed 3 times (3 × 50 mL) with water to remove the supporting electrolyte. The organic solvent was evaporated and the crude mixture, which bears the BF_4^- counter-anion as attested by ^{19}F NMR analysis, was eluted with CH_3CN through an anion exchange resin (AMBERLIT^{TM} IRA96 resin) previously saturated with PF_6^- anions. The solvent was then removed under vacuum. The product was purified by column chromatography (SiO_2, CH_2Cl_2/CH_3OH (9:1, v/v)). Two fractions were collected containing traces of **Zn-8** (Fraction 1) and **Zn-8$^+$,PF$_6^-$** (Fraction 2). Fraction 2 was evaporated then recrystallized in a CH_2Cl_2/*n*-hexane mixture. The precipitate obtained was washed with *n*-hexane and dried at 150 °C under vacuum for 4.25 h to give **Zn-8$^+$,PF$_6^-$** in 56% yield (33.11 mg, 37.5 µmol). ^{1}H NMR ($(CD_3)_2SO$, 500 MHz, 298 K): δ (ppm) 10.34 (d, $^3J_{H\text{-}H}$ = 6.6 Hz, 1H), 9.78 (d, $^3J_{H\text{-}H}$ = 4.7 Hz, 1H), 9.74 (d, $^3J_{H\text{-}H}$ = 4.7 Hz, 1H), 9.62 (s, 1H), 9.42 (d, $^3J_{H\text{-}H}$ = 4.7 Hz, 1H), 8.88-8.79 (m, 3H), 8.51 (d, $^3J_{H\text{-}H}$ = 8.6 Hz, 1H), 8.38 (br dd, 1H), 8.29 (br d, 1H), 8.10 (d, $^3J_{H\text{-}H}$ = 7.4 Hz, 2H), 8.08 (d, $^3J_{H\text{-}H}$ = 7.4 Hz, 2H), 8.02 (br dd, 1H), 7.72 (d, $^3J_{H\text{-}H}$ = 7.5 Hz, 2H), 7.67 (d, $^3J_{H\text{-}H}$ = 7.5 Hz, 2H), 7.39 (m, 1H), 7.03 (dd, $^3J_{H\text{-}H}$ = 7.4 Hz, $^4J_{H\text{-}H}$ = 4.9 Hz, 1H), 6.54 (d, $^3J_{H\text{-}H}$ = 8.4 Hz, 1H), 2.76 (s, 3H), 2.71 (s, 3H); $^{13}C\{^1H\}$ NMR ($(CD_3)_2SO$, 151 MHz, 298 K): δ (ppm) 164.3, 156.6, 156.3, 151.4, 150.2, 149.6, 149.2, 147.1, 146.7, 142.1, 139.8, 138.5, 138.2, 137.3, 137.2, 134.9, 134.8, 134.6, 134.3, 134.1, 133.3, 133.0, 132.5, 129.7, 128.0, 127.5, 123.3, 121.5, 121.0, 21.3, 21.1, 18.6; ^{19}F NMR ($(CD_3)_2SO$, 470 MHz, 298 K): δ (ppm) -70.15 (d, $^1J_{F\text{-}P}$ = 711.4 Hz); ^{31}P NMR ($(CD_3)_2SO$, 202 MHz, 298 K): δ (ppm) -144.19 (hept, $^1J_{P\text{-}F}$ = 711.0 Hz); R_f 0.48

(SiO_2, CH_2Cl_2/CH_3OH (9:1, v/v)); λ_{max} (CH_2Cl_2) / nm (log ε): 319 (4.50), 434 (5.26), 581 (4.10), 631 (3,99); HRMS (ESI+): *m/z* cald for $C_{44}H_{29}N_6S_2Zn^+$ $[M–PF_6]^+$ 769.11811, found 769.11860.

Doubly-fused [5,15-Bis(pyridin-2-ylthio)-10,20-bis(*p*-tolyl)porphyrinato] zinc(II) anti-Zn-8^{2+},2BF$_4^-$. *Electrochemical oxidation.* Zn-8 (40.20 mg, 5.15×10^{-2} mmol, 1.0 eq.) was dissolved in 20 mL of 0.1 M $TEABF_4$ CH_2Cl_2/CH_3CN (4:1) mixture. To improve the solubility of **Zn-8**, pyridine (4.18 µL, 1 eq.) was added, then K_2CO_3 (28.63 mg, 2.07×10^{-1} mmol, 4 eq.) was added. The electrolysis was carried out under an argon atmosphere under vigorous stirring at room temperature and at controlled potential (1.08 V/SCE). Electrolysis was stopped after an uptake of 4.0 F/mol of **Zn-8**. The solvent was removed by rotary evaporation. The crude solid was dissolved in CH_2Cl_2 and washed 3 times with water (3×100 mL) to remove the supporting electrolyte. After evaporation of the solvent, the remaining solid was dissolved in a mixture containing 5 mL of CH_2Cl_2, 1 mL of pyridine and 1 mL of *n*-heptane. Evaporation of CH_2Cl_2 led to the crystallization of the product in the remaining pyridine/*n*-heptane mixture. The crystals were filtered providing **anti-Zn-8^{2+},2BF$_4^-$** in 55% yield (27.02 mg, 2.86×10^{-2} mmol). ^{1}H NMR ($(CD_3)_2CO$, 500 MHz, 298 K): δ (ppm): 10.02 (d, $^3J_{H\text{-}H}$ = 4.5 Hz, 2H), 9.69 (s, 2H), 9.13 (br d, 2H), 9.00 (d, $^3J_{H\text{-}H}$ = 4.2 Hz, 2H), 8.41 (br dd, 2H), 8.28 (br d, 4H), 8.14 (br d, 2H), 8.06 (br dd, 2H), 7.83 (d, $^3J_{H\text{-}H}$ = 7.3 Hz, 4H), 2.89 (s, 6H); $^{13}C\{^1H\}$ NMR ($(CD_3)_2CO$, 600 MHz, 298 K): 150.6, 148.0, 146.2, 145.1, 140.8, 139.0, 138.3, 138.1, 135.6, 134.7, 131.6, 128.3, 126.5, 126.4, 124.1, 124.0, 117.7, 20.9; λ_{max} (DMSO) / nm (log ε): 306 (4.89), 443 (5.59), 460 (5.51), 558 (4.12), 600 (4.35), 641 (4.73), 661 (4.67); HRMS (ESI+): m/z cald for $C_{44}H_{28}N_6S_2Zn^{2+}$ $[M-2BF_4^-]^{2+}$ 384.05487, found 384.05457.

Mono-fused-bis-*meso*,*meso*-linked-[5-(Pyridin-2-ylthio)-10,20-bis(*p*-tolyl)porphyrinato] zinc(II) (Zn-7)$_2^+$,BF$_4^-$. (Zn-7)$_2$ (40.04 mg, 2.372×10^{-2} mmol, 1.0 eq., the molecular weight of

(Zn-7)$_2$ was calculated with 4.6 eq. of pyridine (*M.W.* = 1688.0932 g.mol^{-1}), in agreement with the ^{1}H NMR of **(Zn-7)$_2$** in DMSO, Figure S18) was dissolved in 24 mL of 0.1 M $TEABF_4$ CH_2Cl_2/CH_3CN (4:1) mixture. To improve the solubility of **(Zn-7)$_2$**, pyridine (3.8 µL, 2.0 eq.) was added. The electrolysis was carried out under an argon atmosphere under vigorous stirring at room temperature and at controlled potential (E_{app} = 0.92 V/SCE). Electrolysis was stopped after an uptake of 2.2 F/mol of porphyrin and the solvent was removed by rotary evaporation. The crude solid was dissolved in CH_2Cl_2 and washed three times (3×100 mL) with water to remove the supporting electrolyte. The product was purified by column chromatography (SiO_2, CH_2Cl_2 containing 5% CH_3OH and 1% pyridine). The fractions containing **(Zn-7)$_2^+$,BF$_4^-$** were gathered, solvents were evaporated and the remaining solid was recrystallized in CH_2Cl_2/*n*-heptane and dried under vacuum at 180 °C for 2 h to give **(Zn-7)$_2^+$,BF$_4^-$** in 57% yield (19.16 mg, 1.352×10^{-2} mmol, the molecular weight of **(Zn-7)$_2^+$,BF$_4^-$** was calculated with 0.08 molecule of pyridine (*M.W.* = 1416.3478 g.mol^{-1}, in agreement with the ^{1}H NMR spectrum of **(Zn-7)$_2^+$,BF$_4^-$** in DMSO-d_6, Figure S46). ^{1}H NMR ($(CD_3)_2SO$, 500 MHz, 298 K): δ (ppm): 10.71 (br d,1H), 9.93 (s, 1H), 9.85 (d, $^3J_{H\text{-}H}$=4.4 Hz, 2H), 9.79 (br d, 1H), 9.08 (br d, 1H), 8.98 (br d,1H), 8.88 (d, $^3J_{H\text{-}H}$ =4.5 Hz, 2H), 8.67 (br dd, 1H), 8.55 (m, 2H), 8.51 (d, $^3J_{H\text{-}H}$ =4.0 Hz, 2H), 8.43 (br d, 1H), 8.27 (br dd, 1H), 8.13 (d, $^3J_{H\text{-}H}$ =7.2 Hz, 1H), 8.08 (masked d, 2H), 8.05 (d, $^3J_{H\text{-}H}$ =7.8 Hz, 4H), 7.93 (m, 4H), 7.61 (d, $^3J_{H\text{-}H}$ =7.2 Hz, 2H), 7.55 (d, $^3J_{H\text{-}H}$ =7.4 Hz, 2H), 7.50 (d; $^3J_{H\text{-}H}$ =7.3 Hz, 4H), 7.28 (br dd, 1H), 7.02 (br dd, 1H), 6.18 (d, $^3J_{H\text{-}H}$ =8.0 Hz, 1H), 2.63 (s, 3H), 2.59 (s, 3H), 2.56 (s, 6H). $^{13}C\{^1H\}$ NMR ($(CD_3)_2SO$, 500 MHz, 298 K): 165.7, 156.2, 154.6, 154.4, 151.1, 151.0, 150.1, 149.9, 149.8, 149.5, 148.7, 147.0, 143.1, 140.9, 139.7, 139.3, 139.1, 137.6, 137.5, 137.2, 136.7,135.7, 135.0, 134.6, 133.9, 133.6, 133.3, 132.2, 132.0, 131.0, 128.4, 127.8, 127.7, 124.4, 124.1, 122.6, 122.2, 121.5, 121.4, 120.1, 119.7, 116.9, 105.5, 104.4, 21.6, 21.4. λ_{max} (DMSO)/

nm (log ε): 319 (4.99), 436 (5.63), 471 (5.64), 568 (4.85), 585 (4.87), 633 (4.81); HRMS (ESI+): m/z cald for $C_{78}H_{51}N_{10}S_2Zn_2^+$ $[M-BF_4^-]^+$ 1319.2317, found 1319.2328.

Difused-bis-*meso*,*meso*-linked-[5-(Pyridin-2-ylthio)-10,20-bis(*p*-tolyl)porphyrinato] zinc(II) (Zn-7)$_2^{2+}$,2BF$_4^-$. (Zn-7)$_2$ (40.02 mg, 2.371×10^{-2} mmol, 1.0 eq., the molecular weight of **(Zn-7)$_2$** was calculated with 4.6 eq. of pyridine (*M.W.* = 1688.0932 g.mol^{-1}), in agreement with the ^{1}H NMR of **(Zn-7)$_2$** in DMSO, Figure S18) was dissolved in 24 mL of 0.1 M $TEABF_4$ CH_2Cl_2/CH_3CN (4:1) mixture. To improve the solubility of **(Zn-7)$_2$**, pyridine (4 µL, 2.0 eq.) was added. The electrolysis was carried out under an argon atmosphere under vigorous stirring at room temperature and at controlled potential (E_{app} = 0.92 V/SCE. Electrolysis was stopped after an uptake of 4.8 F/mol of **(Zn-7)$_2$** and the solvent was removed by rotary evaporation. The crude solid was dissolved in CH_2Cl_2 and washed 3 times (3×100 mL) with water to remove the supporting electrolyte. The product was purified by column chromatography (SiO_2, CH_2Cl_2 containing 5% CH_3OH and 1% pyridine). The fractions containing **(Zn-7)$_2^{2+}$,2BF$_4^-$** were gathered, solvents were evaporated and the remaining solid was recrystallized in CH_2Cl_2/*n*-heptane and dried at 180 °C for 2h to give **(Zn-7)$_2^{2+}$,2BF$_4^-$** in 98% yield (35.10 mg, 2.335×10^{-2} mmol, the molecular weight of **(Zn-7)$_2^{2+}$,2BF$_4^-$** was calculated with 0.09 molecule of pyridine (*M.W.* = 1502.9344 g.mol^{-1}), in agreement with the ^{1}H NMR spectrum of **(Zn-7)$_2^{2+}$,2BF$_4^-$** in DMSO, Fig. S52). ^{1}H NMR ($(CD_3)_2SO$, 500 MHz, 298 K): δ (ppm) 10.72 (d, $^3J_{H-H}$ = 6.2 Hz, 2H), 9.94 (s, 2H), 9.80 (d, $^3J_{H-H}$ = 4.5 Hz, 2H), 9.07 (d, $^3J_{H-H}$ = 8.5 Hz, 2H), 8.99 (d, $^3J_{H-H}$ = 4.5 Hz , 2H), 8.67 (br dd, 2H), 8.60 (d, $^3J_{H-H}$ = 4.5 Hz, 2H), 8.59 (d, $^3J_{H-H}$ = 4.5 Hz, 2H), 8.27 (br dd, 2H), 8.14 (d, $^3J_{H-H}$ = 7.5 Hz, 4H), 8.09 (d, $^3J_{H-H}$ = 7.5 Hz, 4H), 7.99 (d, $^3J_{H-H}$ = 4.5 Hz, 2H), 7.94 (d, $^3J_{H-H}$ = 4.5 Hz, 2H), 7.63 (d, $^3J_{H-H}$ = 7.7 Hz, 4H), 7.56 (d, $^3J_{H-H}$ = 7.6 Hz, 4H), 2.64 (s, 6H), 2.60 (s, 6H). $^{13}C\{^1H\}$ NMR ($(CD_3)SO$, 500 MHz, 298 K): δ (ppm) 155.9, 155.8, 150.5, 149.5, 149.3,

148.2, 146.6, 142.7, 140.8, 140.5, 138.8, 138.6, 137.14, 137.09, 135.3, 134.6, 134.1, 134.0, 133.5, 133.2, 133.0, 130.6, 127.9, 127.4, 127.0, 125.7, 124.0, 123.7, 121.8, 118.8, 116.5, 105.2, 21.1, 21.0; λ_{max} (DMSO)/nm (log ε): 319 (4.77), 449 (5.22), 476 (5.41), 548 (4.24), 591 (4.50), 638 (4.62); HRMS (ESI+): m/z cald for $C_{78}H_{51}N_{10}S_2Zn_2^{2+}$ $[M-2BF_4]^{2+}$ 659.1117, found 659.1142.

RESULTS AND DISCUSSION

Synthesis and characterization of unfused porphyrins Zn-6, Zn-7 and Zn-8.

The synthesis of the unfused porphyrins **Zn-6**, **Zn-7** and **Zn-8** is depicted in Scheme 1 and is close to the one previously reported for the nickel(II) analogues.[23] Briefly, **3** and **4** were prepared *via* bromination of 5,15-bis(*p*-tolyl)-10-phenylporphyrin **1** and 5,15-bis(*p*-tolyl)porphyrin **2** with 1.2 and 0.8 eq. of *N*-bromosuccinimide (NBS), respectively. For the synthesis of **4** a substoichiometric amount of NBS was used to favor the monobromination. Thus, starting from **2**, a mixture of **2** (28%), **4** (60%) and **5** (12%) that was not possible to purify was obtained (yields estimated from ^{1}H NMR analysis). The bis-*meso*-brominated free-base porphyrin **5** was more efficiently synthesized from **2** after zinc(II) metalation (**Zn-2**), dibromination (**Zn-5**) and finally demetalation with trifluoroacetic acid (**5**).[58] The next step consisted in the aromatic nucleophilic substitution (S_NAr)[66–72] of the bromine atom with 2-mercaptopyridine.[55] The free-base porphyrins **6**, **7** and **8** were obtained in 78, 61 and 68% yield, respectively. Final quantitative zinc(II) insertion into these free-bases afforded the unfused porphyrins **Zn-6**, **Zn-7** and **Zn-8**.

Scheme 1. Synthesis of porphyrins **Zn-6**, **Zn-7** and **Zn-8**.

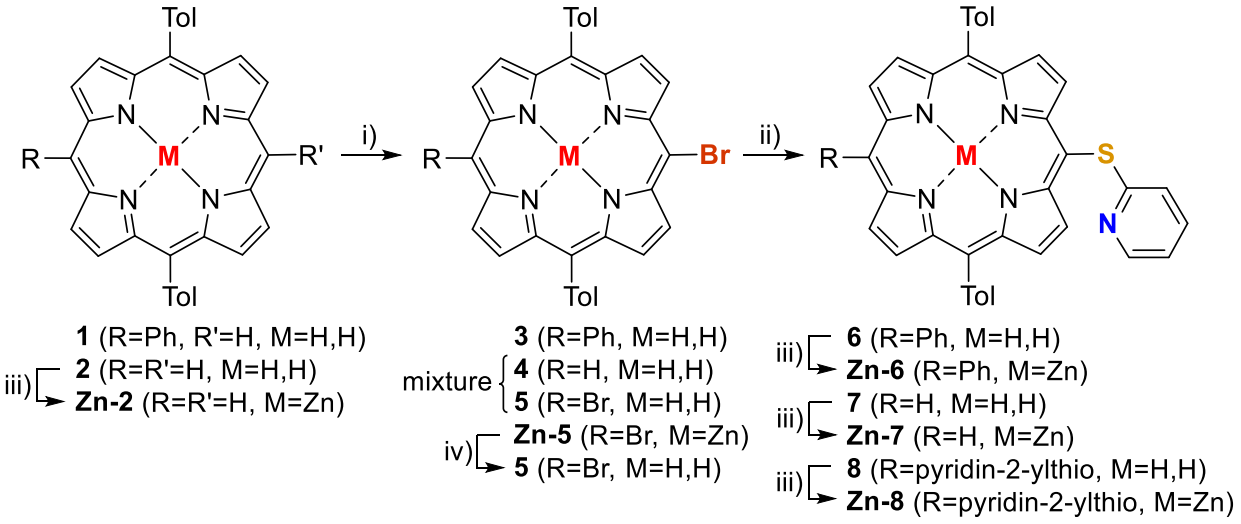

Conditions: i) NBS, $CHCl_3$, pyridine, 0 °C; ii) 2-mercaptopyridine, Cs_2CO_3, DMF, 100 °C, Ar; iii) $Zn(OAc)_2.2H_2O$ (2 eq.), $CHCl_3$/MeOH, 60 °C; iv) TFA/CH_2Cl_2

Zn-6, **Zn-7** and **Zn-8** were fully characterized by NMR, HRMS, UV-vis absorption spectroscopy, cyclic voltammetry and for **Zn-7** and **Zn-8**, by X-ray crystallography. The crystallographic structure of the free-base **7** is also presented in this manuscript.

For **Zn-6**, **Zn-7** and **Zn-8**, non-soluble coordination polymers may form in non-coordinating solvent due to the intermolecular coordination of the pyridinyl moiety on the zinc(II) atom of another porphyrin. This assertion is supported by molecular modeling for **Zn-6** and **Zn-8** (see Figures S90 and S91) as well as by the X-ray crystallographic structure of **Zn-8** (see below). The formation of pyridinyl-zinc(II)-porphyrin-based coordination oligomers and polymers have already been reported in the literature.[73–84] The most common examples concern tetramer[73–82] but polymer[83] and double-stranded coordination helices have also been reported.[84] Thus NMR analyses were performed with coordinating solvents ($(CD_3)_2CO$/pyridine-d_5 mixture or $(CD_3)_2SO$) to reach a sufficiently high concentration of these zinc(II) complexes in solution as well as to improve the resolution of the signals. Indeed, these ^1H NMR spectra exhibit common features with four signals attributed to the pyridinyl fragments between 5.90 and 8.40 ppm, two

(**Zn-8**) or four (**Zn-6** and **Zn-7**) β-pyrrolic doublets between 8.81 and 9.88 ppm, two doublets for the CH-tolyl fragments between 7.58 and 8.08 ppm and one singlet attributed to the methyl group between 2.64 and 2.68 ppm (see the ^{1}H NMR spectrum of **Zn-8** in Figure 1, top, as an illustrating example).

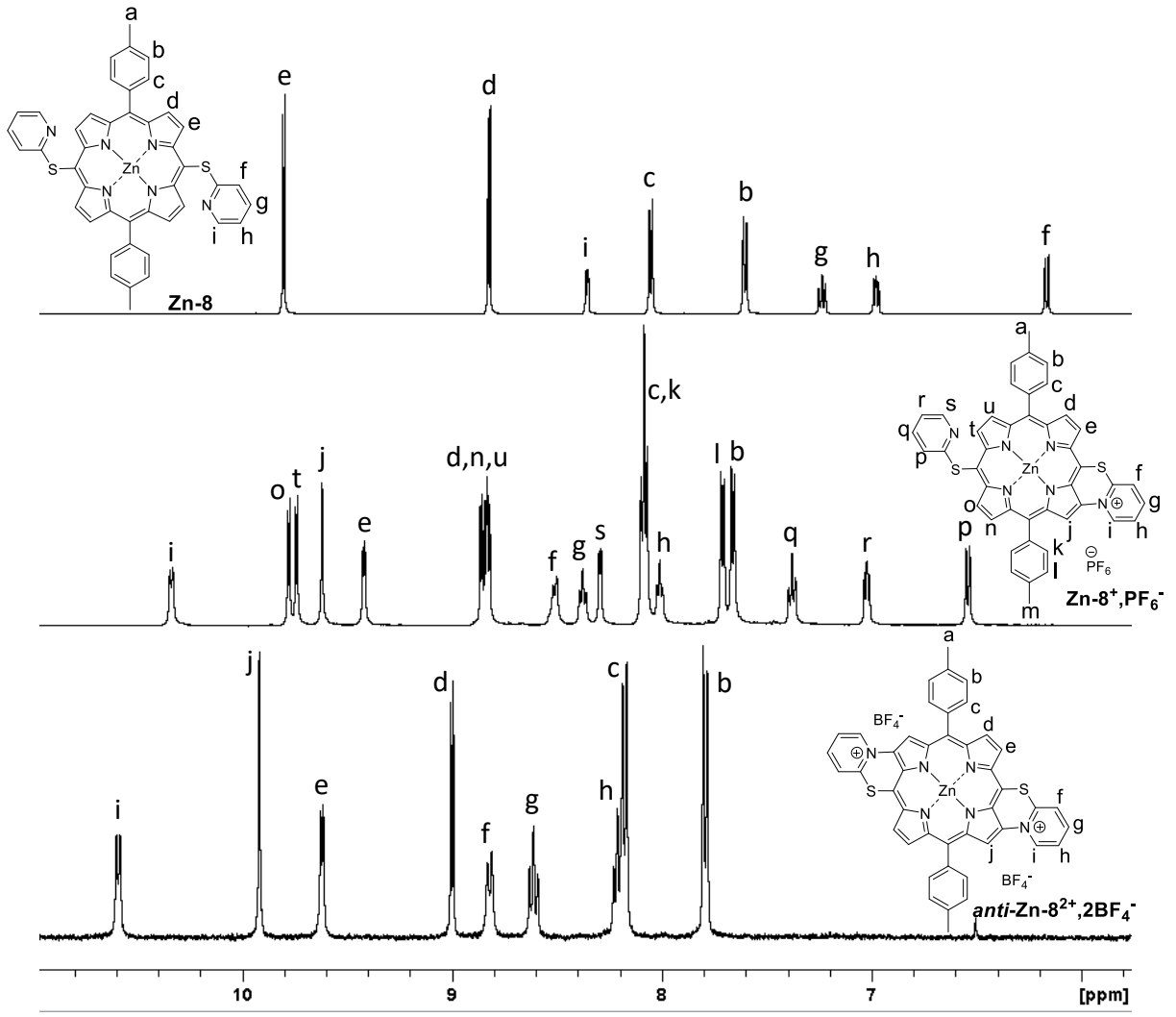

Figure 1. Partial ^{1}H NMR spectra of **Zn-8** (top), **Zn-8^{+},PF$_6^-$** (middle) and **Zn-8^{2+},2BF$_4^-$** (bottom). Conditions: $(CD_3)_2SO$, 500 MHz, 300 K.

The X-ray crystallographic structures of **7**, **Zn-7** and **Zn-8** are presented in Fig. 2-4 and additional views are shown in Fig. S83-S84 for **Zn-8**. For these molecules, the RMS deviation,

which was calculated with the 24 C and N atoms of the porphyrin ring is 0.0974, 0.1146 and 0.1766 Å, respectively. The C_{meso}-S distance(s) are 1.785(3), 1.778(2), 1.770(3) and 1.772(3) Å, respectively which are comparable with other *meso*-S-porphyrins[85,86,70,87] ($1.754 \leq d(C_{meso}\text{-S}) \leq 1.856$ Å) and the analogous nickel(II) complexes **Ni-6** and **Ni-7** (1.772(3) and 1.779(3) Å, respectively).[23] The C_{meso}-S-$C_{pyridine}$ angles measure 103.68(17), 103.09(9), 106.15(16) and 103.19(14)°, respectively, in the same range as those reported for C_{meso}-S-R angles ($101.50 \leq C_{meso}\text{-S-R} \leq 108.22°$, with R = C or S atom).[85,86,70,87] The C_{porph}-C_{meso}-S-$C_{pyridine}$ torsion angles are −71.4(3), −87.50(17), 66.8(4) and 87.3(3)°, respectively. For the zinc(II) complexes **Zn-7** and **Zn-8**, the distance between the zinc(II) atom and the mean plane of the porphyrin is 0.3441(5) and 0.3927(7) Å, respectively, whereas the distance between the metal and the nitrogen atoms from the porphyrins varies from 2.0560(3) to 2.0800(16) Å. **Zn-7** and **Zn-8** are both coordinated by one pyridine moiety coming either from exogenous pyridine added to favor the crystallization process (**Zn-7**, $d(\text{Zn-N}_{pyridine})$ = 2.1392(16) Å) or endogenous thiopyridinyl fragment from another porphyrin molecule (**Zn-8**, $d(\text{Zn-N}_{pyridine})$ = 2.223(3) Å). Interestingly, a triangular-shaped coordination trimer is revealed by the X-ray crystallographic structure of **Zn-8**. Coordination trimers are very rare[81,88,89] and to the best our knowledge the sole pyridinyl-porphyrin-based trimer X-ray crystallographic structure was reported in 2006 by Higuchi, Kim, Osuka and co-workers.[81]

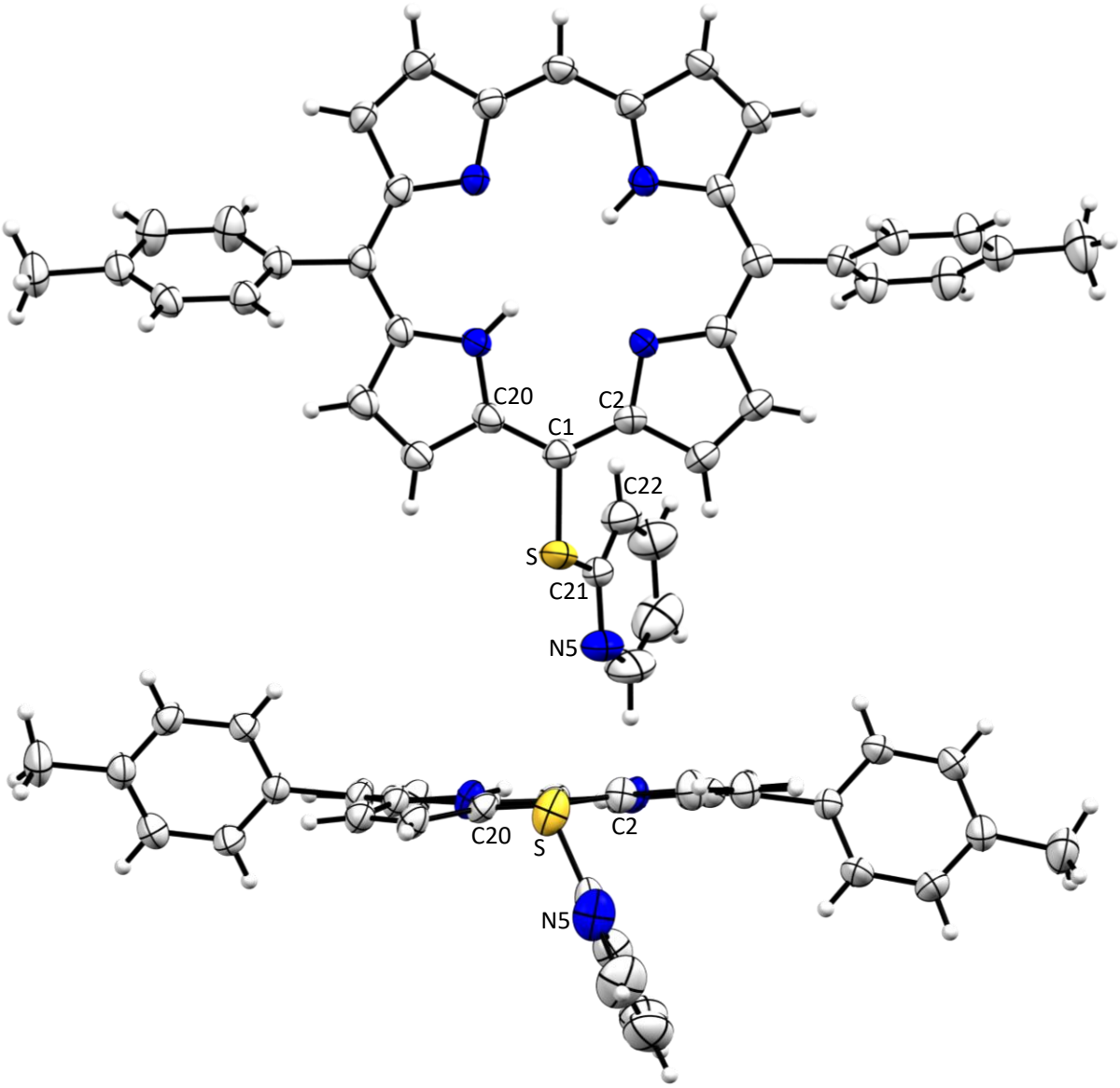

Figure 2. Front (top) and side (bottom) Mercury[90] views of **7**. Thermal ellipsoids are scaled to the 50% probability level.

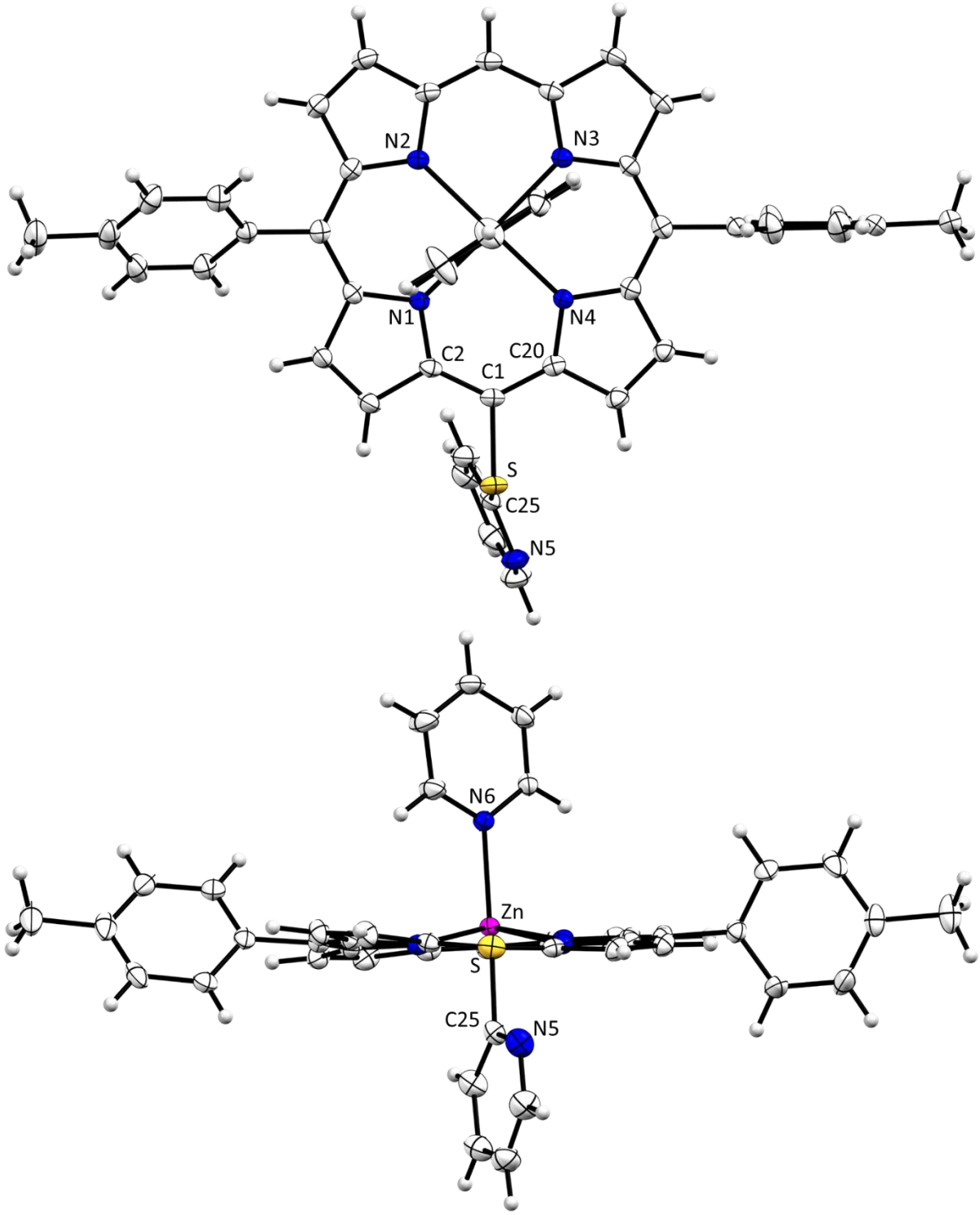

Figure 3. Front (top) and side (bottom) Mercury[90] views of **Zn-7•pyridine**. Thermal ellipsoids are scaled to the 50% probability level.

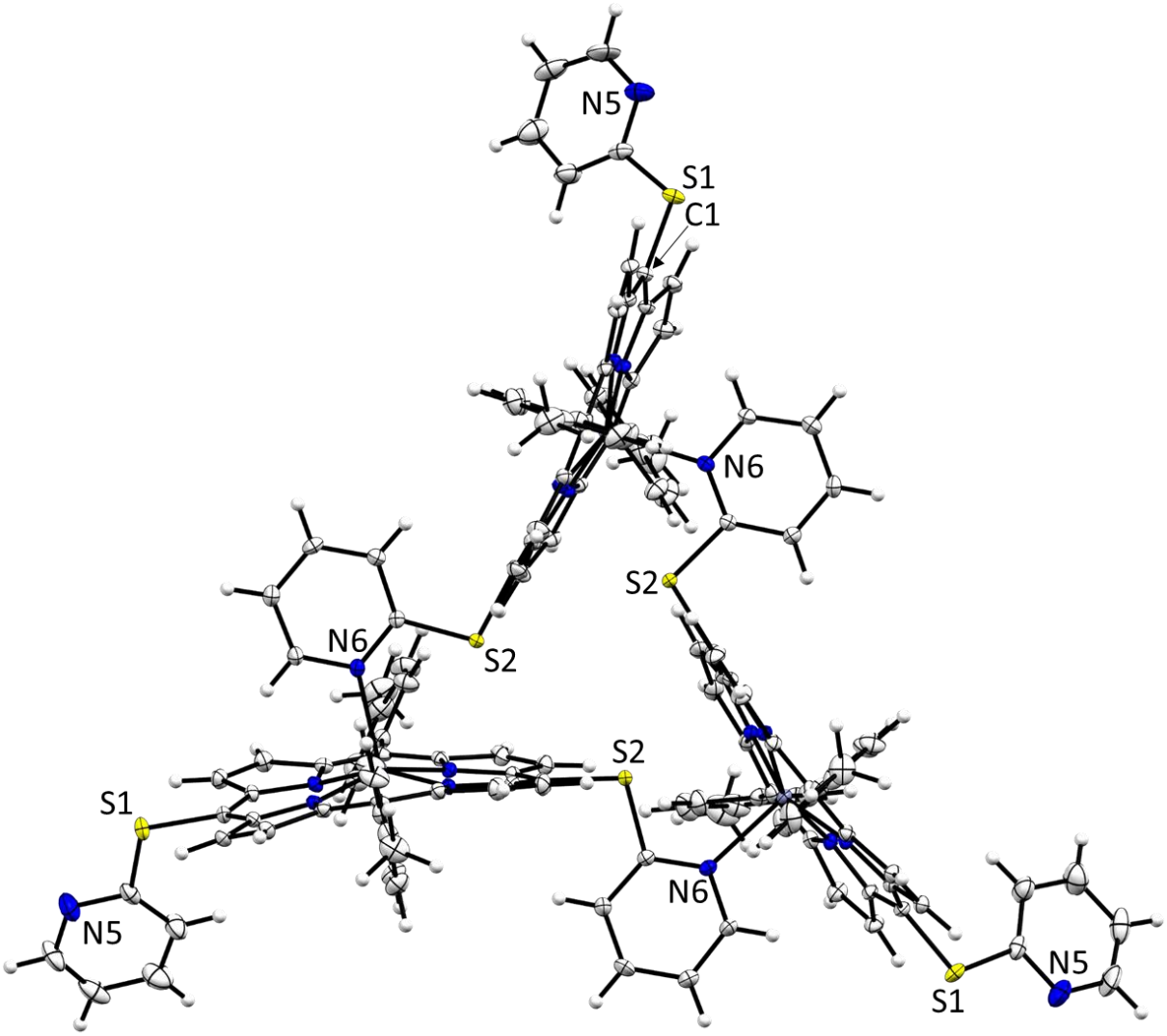

Figure 4. Side Mercury[90] views of **Zn-8** coordination trimer. Thermal ellipsoids are scaled to the 50% probability level. Solvent molecules have been removed for clarity.

The redox properties of **Zn-6**, **Zn-7** and **Zn-8** were assessed by cyclic voltammetry (CV) in CH_2Cl_2 0.1 M tetra-*n*-butylammonium hexafluorophosphate ($TBAPF_6$, see Figure 5). All the potentials mentioned in this manuscript are given *vs* the KCl saturated calomel electrode (SCE). The porphyrins were only partially soluble at 10^{-3} M in this non-coordinating solvent. However, the addition of one equivalent of pyridine led to the full solubilization of the zinc(II) complexes. In the negative potential range, these unfused porphyrins show commonly observed reversible

mono-electronic reduction peak which corresponds to the first ring-centered reduction (formation of the porphyrin anion radical).[91] However, in the positive potential range, the first oxidation system is not fully reversible for **Zn-6** ($i_{pc}/i_{pa} \approx 0.3$) and totally irreversible for **Zn-7** and **Zn-8** which indicates that the electrogenerated porphyrin cation radicals are not stable on the CV time scale and undergo subsequent chemical reaction(s).

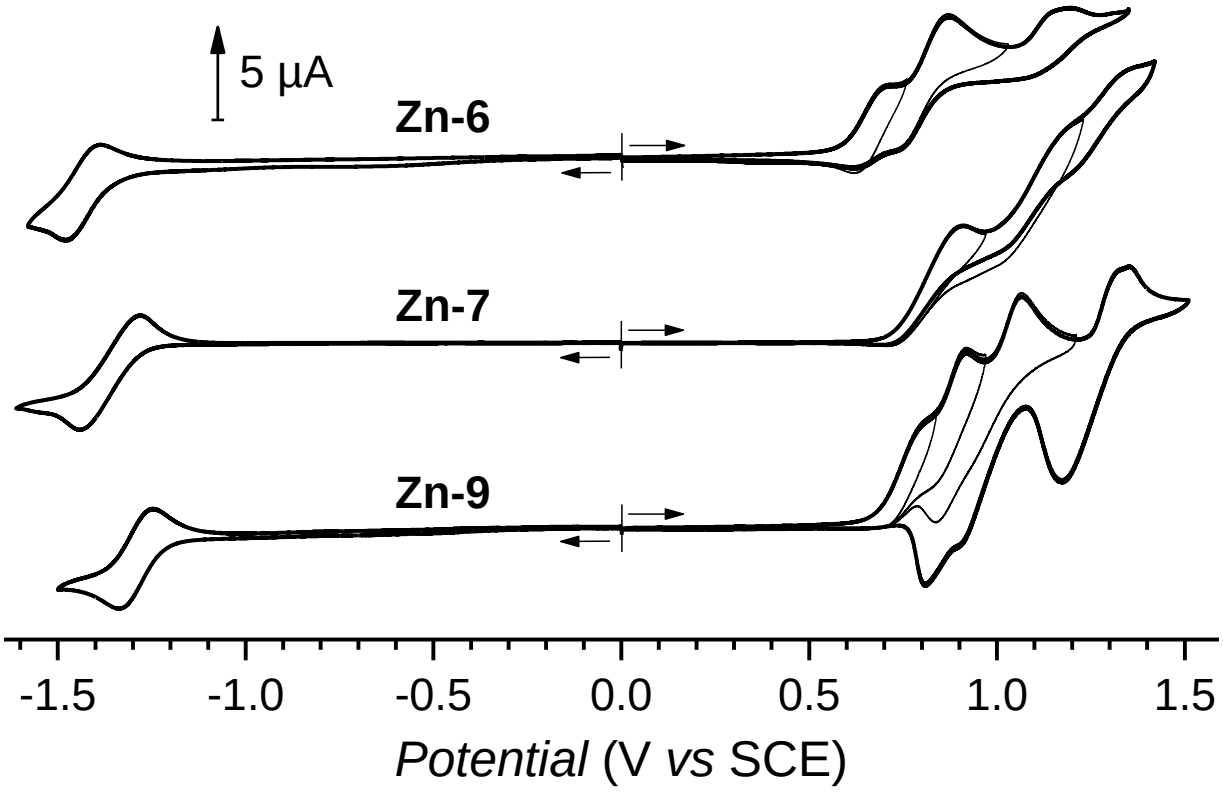

Figure 5. Cyclic voltammograms of **Zn-6**, **Zn-7**, and **Zn-8** (CH_2Cl_2 0.1 M $TBAPF_6$ + 1.0 equiv. of pyridine, $c = 10^{-3}$ M, $v = 100$ mV s^{-1}, WE: Pt, $\varnothing = 2$ mm).

Oxidative C-N fusion of porphyrins Zn-6 and Zn-8 and characterization of the C-N fused compounds.

Scheme 2. Synthesis of **Zn-6**$^{+}$, **Zn-8**$^{+}$ and ***anti*-Zn-8**$^{2+}$ *via* intramolecular C-N oxidative coupling.

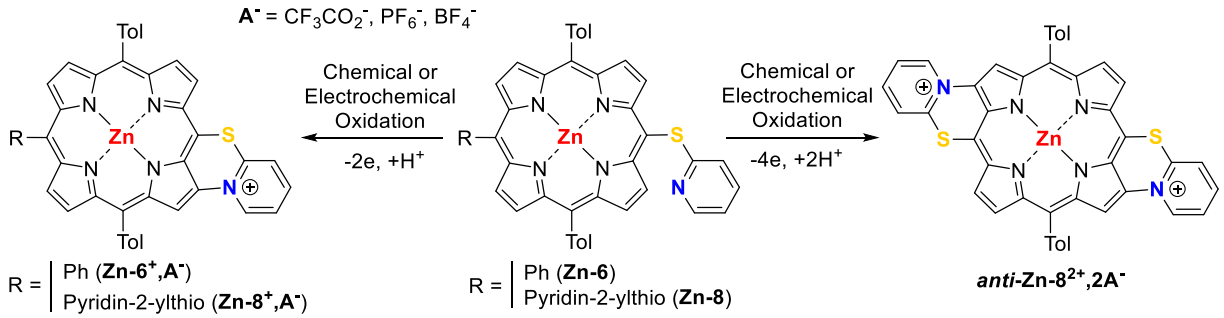

Previous researches on the analogous nickel(II) complexes demonstrated that bis(trifluoroacetoxy)iodo)benzene (PIFA) was the most efficient oxidant for the C-N oxidative coupling reaction.[23] These optimized conditions (1.0 eq. PIFA in CH_2Cl_2 at room temperature during 1 h) were first reproduced on the zinc(II) complexes **Zn-6**. The C-N fused cation **Zn-6**$^{+}$**,CF$_3$CO$_2$**$^{-}$ (Scheme 2, the trifluoroacetate anion is released from PIFA during its reduction) was obtained in 61% along with some demetalated fused derivative. To avoid the demetalation process and favor the solubility of the porphyrin **Zn-6**, 1.0 eq. of pyridine was added as a base using the same previous conditions. In this case, only traces of the fused target **Zn-6**$^{+}$**,CF$_3$CO$_2$**$^{-}$ were detected. Possibly, interaction of pyridine with the iodonium cation of PIFA may lead to a decrease of its oxidizing power.[28] This assertion is supported by the fact that the C-N fusion can be performed electrochemically, in presence of pyridine (see below). We thus considered K_2CO_3 as a base. Replacing pyridine by 2 eq. of K_2CO_3 mainly afforded the target **Zn-6**$^{+}$**,CF$_3$CO$_2$**$^{-}$ compound with only traces of the precursor **Zn-6**. A slight excess of PIFA (1.2 eq.) and 2 h reaction time were therefore required for an exhaustive transformation of **Zn-6** into **Zn-6**$^{+}$**,CF$_3$CO$_2$**$^{-}$. To make the purification easier on silica gel column chromatography, the $CF_3CO_2^-$ anion was exchanged for PF_6^- using an anion exchange resin - the fused compound is much less

polar with the hexafluorophosphate anion - which afforded **Zn-6^{+},PF$_6^-$** in 91% isolated yield. Applying the same optimized conditions to **Zn-8** provided the mono C-N fused derivative **Zn-8^{+},PF$_6^-$** (Scheme 2) in 60% isolated yield. It was not possible to reach a better selectivity since a decrease in the amount of PIFA increased the amount of starting porphyrin **Zn-8** while an increase favored the formation of the doubly C-N fused derivative **Zn-8^{2+},2CF$_3$CO$_2^-$** as noticed by TLC (green polar spot) and ^{1}H NMR analysis of the crude reaction mixture. Interestingly, the very low number of signals observed for **Zn-8^{2+},2CF$_3$CO$_2^-$** as well as the occurrence of only one singlet (6H, methyl group) at 2.89 ppm (in deuterated acetone) agrees well with the unique formation of the *anti*- regioisomer ***anti*-Zn-8^{2+},2CF$_3$CO$_2^-$** (Scheme 2), as previously observed by Kim, Osuka and co-workers.[92] In our former communication,[23] theoretical studies on the C–N bond formation with **Ni-8** revealed that the *anti* isomer was favored both kinetically and thermodynamically. Indeed, the SOMO of **Ni-8** cation radical **(Ni-8^{+})** presented a large coefficient on the *anti* β-position, while no electronic density was observed on the *syn* β-position. It is expected that the zinc(II) complex behaves similarly. The selective synthesis of the dication **Zn-8^{2+},2CF$_3$CO$_2^-$** was attempted from **Zn-8** by almost doubling the amount of oxidant that was used for the monofusion reaction (2.0 eq. of PIFA) and increasing the reaction time up to 14 h. In these conditions, **Zn-8^{+},CF$_3$CO$_2^-$** was still present in the reaction mixture. The amount of PIFA was thus gradually increased up to 5 eq. but the subsequent crude reaction contained a mixture of products resulting from the oxidation of the sulfur atoms (sulfoxide and sulfone) of **Zn-8^{+},CF$_3$CO$_2^-$** and ***anti*-Zn-8^{2+},2CF$_3$CO$_2^-$** as attested by mass spectrometry (+16 and +32 amu). Whatever the reaction and chromatographic conditions (SiO_2 or C_{18} stationary phases), it was not possible to reach a satisfactory purity of either ***anti*-Zn-8^{2+},2CF$_3$CO$_2^-$** or ***anti*-Zn-8^{2+},2PF$_6^-$**.

To compare the electrochemical route to the chemical one, the oxidative C-N fusion of **Zn-6** and **Zn-8** was also performed by electrosynthesis in CH_2Cl_2 0.1 M tetraethylammonium tetrafluoroborate ($TEABF_4$) in the presence of 2 eq. (4.0 eq. for the double C-N fusion) of K_2CO_3 (used as a base) and pyridine (1-2 eq., used to improve the solubility of the Zn(II) porphyrins). Applying a potential corresponding to the first oxidation peak of the porphyrin (formation of the porphyrin cation radical) and after abstraction of 2.0 F/mol *vs* the porphyrin, the crude solution was analyzed by CV and then submitted to water washing to remove the supporting electrolyte. As a first evidence that the C-N fusion reaction worked, a new irreversible reduction peak was observed near −0.8/−1.0 V (E_{pc}(R1) = −0.97 V on the CV of **Zn-8**$^+$**,PF$_6^-$**, Fig. 6). This potential range is typical of pyridinium reduction,[25,27,31,32] in particular for C-N fused porphyrin cations.[23] The MALDI-TOF mass spectrometry analysis of the crude solution resulting from the oxidation of **Zn-6** and **Zn-8** showed the expected **Zn-6**$^+$ (*m*/z = 736.1508) and **Zn-8**$^+$ (*m*/z = 768.1181) peaks, with a perfect match of their respective isotopic pattern. Previous studies with the nickel(II) counterpart of **Zn-8** (**Ni-8**) evidenced the very high chemical and electrochemical selectivity of the C-N fusions reactions for the C-N oxidative reaction.[23] This high selectivity lies on the significant potential difference observed for the first oxidations of **Ni-8** and **Ni-8**$^+$ (*ca*. +150 mV), *i.e*. the C-N fused derivative was oxidized at a much higher potential than the starting unfused porphyrin. Surprisingly, the first oxidations (peaks O1) of the electrogenerated singly-fused cations **Zn-6**$^+$ and **Zn-8**$^+$ have only small potential difference (< +100 mV) as compared to their respective non-fused porphyrin (E_{pa}(O1) ≈ 0.81 V for **Zn-8** *vs* E_{pa}(O1) ≈ 0.89 V for **Zn-8**$^+$**,PF$_6^-$**, Fig. 6). Therefore, when a potential that corresponds to the first oxidation of the unfused porphyrin is applied, the electrogenerated C-N fused derivative is partially oxidized leading to lower selectivity for the reaction, especially when two consecutive C-N fusion reactions are

possible. The lack of selectivity for the chemical oxidation of **Zn-8** with PIFA certainly arises from this redox behavior.

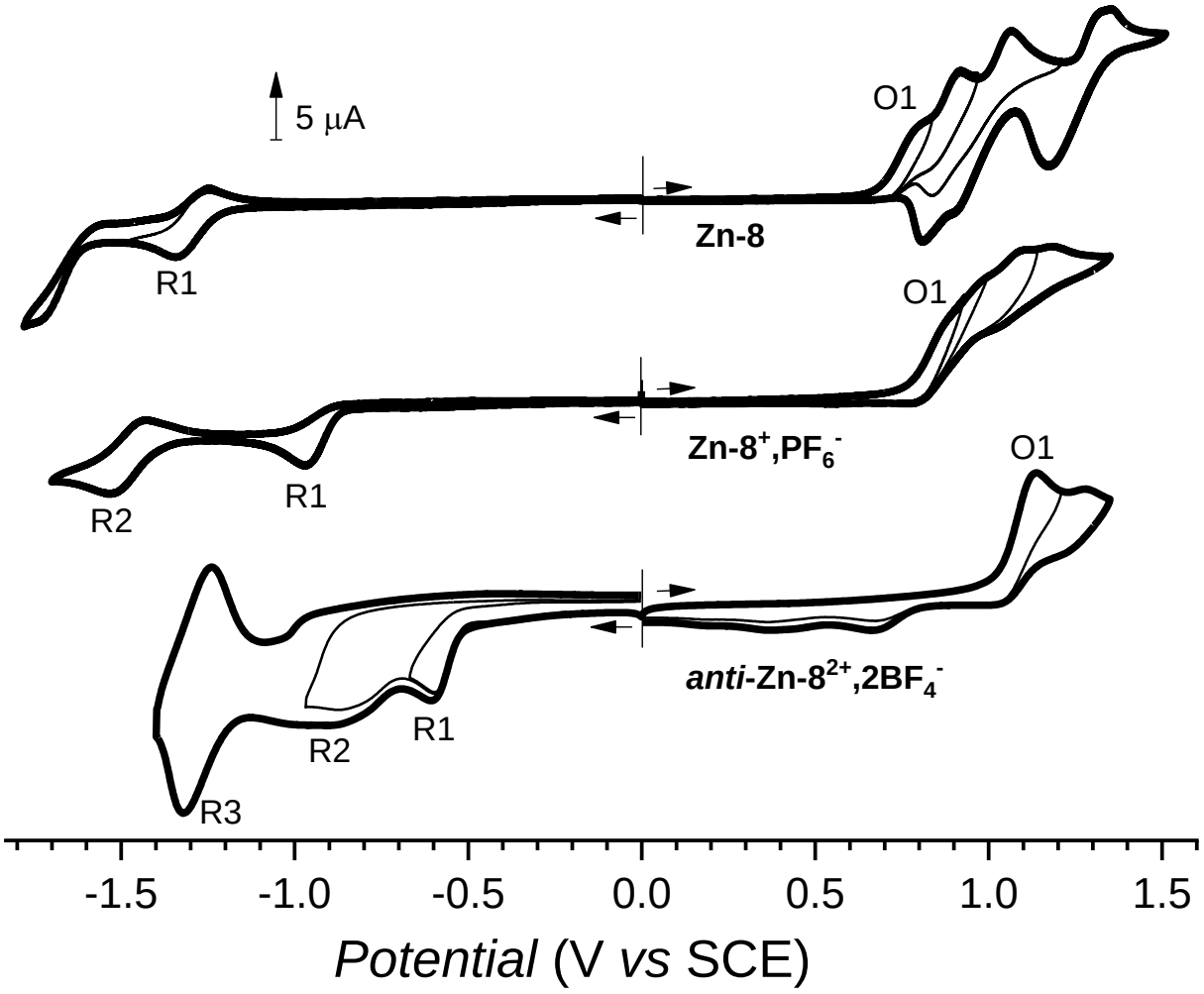

Figure 6. Cyclic voltammograms of **Zn-8**, **Zn-8^{+},PF$_6^-$** (CH_2Cl_2 0.1 M $TBAPF_6$ + 1.0 eq. of pyridine, WE: Pt, $\varnothing$ = 2 mm) and ***anti*-Zn-8^{2+},2BF$_4^-$** (CH_2Cl_2/CH_3CN 4:1 v/v 0.1 M $TEABF_4$ + 1.0 eq. of pyridine, WE: Pt, $\varnothing$ = 1.6 mm), $c = 10^{-3}$ M, v = 100 mV s^{-1}.

To keep the same anion as the one obtained by the chemical pathway, the BF_4^- was exchanged for PF_6^- using an anion exchange resin. **Zn-6^{+},PF$_6^-$** and **Zn-8^{+},PF$_6^-$** were thus obtained in 83 and 56% isolated yield, respectively. With the hope to reach a better selectivity for the formation of the doubly C-N fused ***anti*-Zn-8^{2+}** that could facilitate its purification, oxidation of **Zn-8** was

performed at its second oxidation peak (O2) (E_{app} = 1.07 V, −4.0 F/mol). After removal of the supporting electrolyte and evaporation of the solvents, the crude solid was analyzed by ^{1}H NMR spectroscopy. ***Anti*-Zn-8^{2+},2BF$_4^-$** was the main product (> 80% according to NMR analysis) and was only contaminated with slight amount of **Zn-8$^+$,BF$_4^-$**. Interestingly, no oxidation of the sulfur atoms was noticed either by TLC or by mass spectrometry. A direct crystallization of the crude solid was attempted using a pyridine/CH_2Cl_2/*n*-heptane mixture. Fortunately, ***anti*-Zn-8^{2+},2BF$_4^-$** crystallizes in these conditions which makes it possible to isolate this dicationic product in 55% yield.

The CV of ***anti*-Zn-8^{2+},2BF$_4^-$** confirmed the formation of the bis-pyridinium derivative since two reduction peaks were observed at E_{pc}(R1) = −0.60 and E_{pc}(R2) ≈ −0.87 V (Figure 6). Moreover, the first oxidation potential of ***anti*-Zn-8^{2+},2BF$_4^-$** (E_{pa}(O1) = 1.14 V) is much higher than **Zn-8** and **Zn-8$^+$,PF$_6^-$**, in agreement with the presence of two electron-withdrawing pyridinium fragments.

The ^{1}H NMR spectra analysis of the pure C-N fused porphyrins **Zn-6$^+$,PF$_6^-$** and **Zn-8$^+$,PF$_6^-$** (Figure 1, middle) confirms their loss of symmetry. The β-pyrrolic proton close to the position where the C-N fusion takes place (H_j in Figure 1) appears as a singlet integrating for one proton at 8.71 and 8.62 ppm, respectively. The six other β-pyrrolic doublets integrate each for one proton and appear at different chemical shifts, between 9.8 and 8.8 ppm. As expected, the pyridinium protons undergo an important unshielding as compared to the pyridinyl protons of the initial unfused porphyrin **Zn-8** (see Figure 1 for comparison). For example, the pyridinium protons of **Zn-8$^+$,PF$_6^-$** are observed at 10.33, 8.51, 8.38 and 8.01 ppm whereas the pyridinyl protons of **Zn-8** appears at 8.35, 7.23, 6.88 and 6.16 ppm. These last values are relatively close to the ones found for the unfused pyridinyl moiety of **Zn-8$^+$,PF$_6^-$** (8.28, 7.38, 7.02 and 6.54

ppm). Another typical ^{1}H NMR feature of these singly C-N fused compounds consists in the existence of two singlets integrating each one for 3 H at 2.76 and 2.71 ppm corresponding to the chemically non-equivalent methyl fragments (H_a and H_m in Figure 1). Concerning the doubly-C-N-fused ***anti*-Zn-8^{2+},2BF$_4^-$** derivative, its high symmetry is verified from ^{1}H NMR analyses (Figure 1, bottom). Indeed, the two β-pyrrolic protons close to the position where the C-N fusion takes place (H_j in Figure 1) appear as one singlet at 9.92 ppm. Two β-pyrrolic doublets integrating each for two protons are located at 9.62 and 9.00 ppm. The pyridinium protons are observed at 10.59, 8.82, 8.61 and 8.21 ppm and each signal integrates for two protons. Also consistent with the *anti* symmetry, only one singlet (6H) at 2.81 ppm is seen for the methyl protons whereas only two doublets (4H each) are observed for the C-H tolyl protons at 8.18 and 7.79 ppm.

The fused compounds systematically undergo a bathochromic shift of the Soret and Q bands (see ESI). As an example, the normalized UV-visible absorption spectra of **Zn-8**, **Zn-8$^+$,PF$_6^-$** and ***anti*-Zn-8^{2+},2BF$_4^-$** in DMSO are presented in Figure 7. The more intense B band is shifted from 436 to 439 to 443 nm for **Zn-8**, **Zn-8$^+$,PF$_6^-$** and ***anti*-Zn-8^{2+},2BF$_4^-$**, respectively. Interestingly, a shoulder at *ca.* 451 nm appears on the lower energy side of the Soret band for the mono-C-N fused **Zn-8$^+$,PF$_6^-$** whereas a clear split of the Soret band is observed for ***anti*-Zn-8^{2+},2BF$_4^-$** with a new Soret band at 460 nm ($\Delta\lambda$(Soret bands) = 17 nm). This remarkable splitting behaviour was not observed for the respective nickel(II) complexes.[23] In agreement with a progressive extension of the conjugation, the full width at half maximum (fwhm) is also progressively increasing from 13 nm for the initial unfused **Zn-8** porphyrin to 25 and 33 nm for **Zn-8$^+$,PF$_6^-$** and ***anti*-Zn-8^{2+},2BF$_4^-$** respectively.

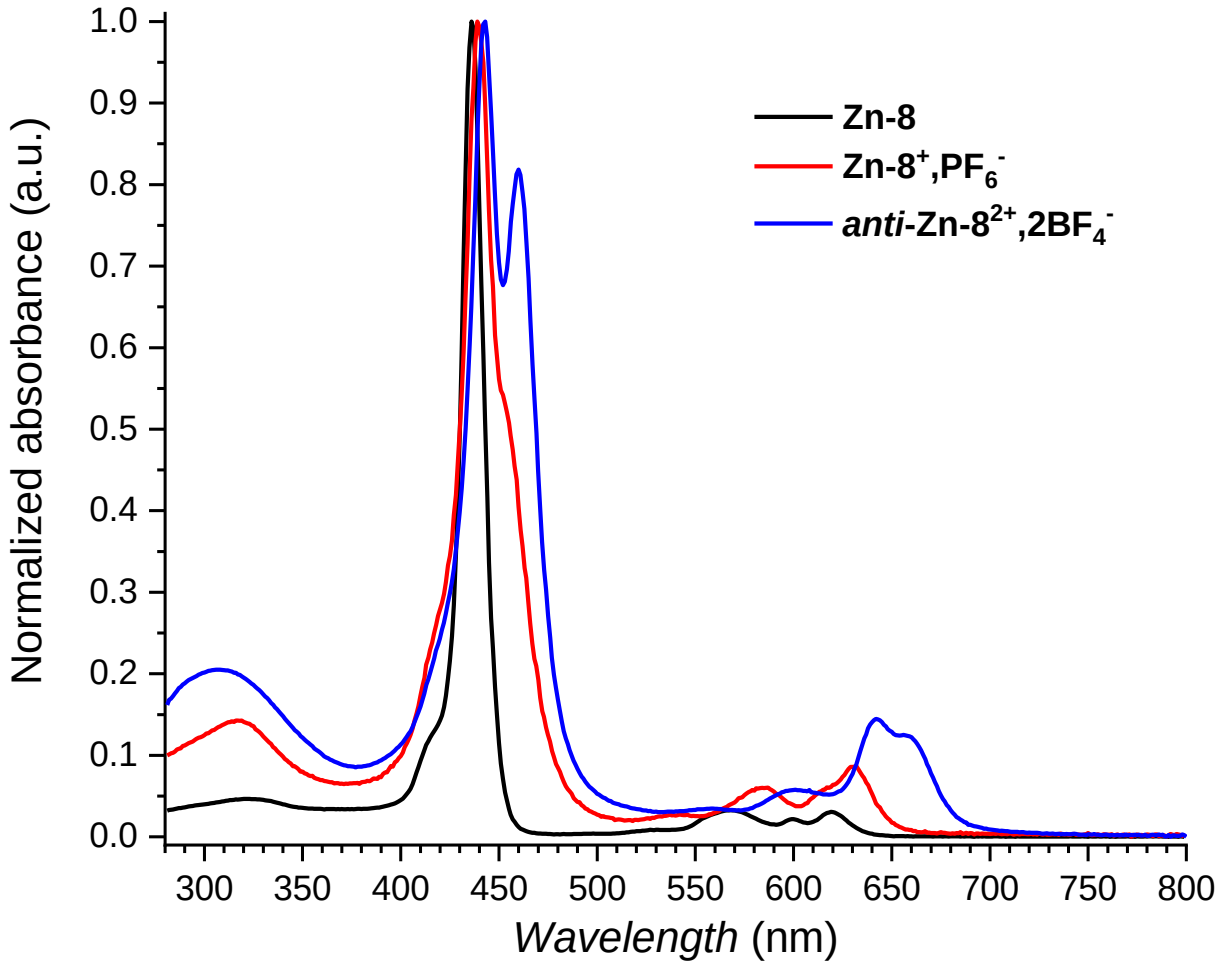

Figure 7. Normalized UV-visible absorption spectra of **Zn-8** (black curve), **Zn-8^{+},PF$_6^{-}$** (red curve) and ***anti*-Zn-8^{2+},2BF$_4^{-}$** (blue curve) in DMSO at room temperature.

The main features of the UV-visible absorption spectra of porphyrins can be explained with the four orbitals model of Gouterman (Figure 8).[93–95] Zinc(II) porphyrins are regular[96] porphyrins, and the **Zn-8** UV-visible absorption spectrum is thus similar to a non metalated porphyrin with multiple peaks for the Q bands and one intense B signal. The thiopyridinyl substituents do not participate to these transitions. After the first C-N fusion, the thiopyridinyl fragment interacts with the porphyrin orbitals. However, this interaction is stronger with the HOMO and LUMO orbitals that have large coefficients on the carbon atoms bearing the thiopyridinyl substituents.

Therefore, the HOMO/LUMO energy difference decreases when moving from **Zn-8** to **Zn-8**$^{+}$ and **Zn-8**$^{2+}$ while the HOMO-1/LUMO+1 energy difference decreases only slightly. Additionally, for the Q_x and B_x bands; another contribution arises from a charge transfer from the porphyrin to the thiopyridinyl moieties. This is responsible for both the wavelengths increases along the C-N fusion and the split of the Soret band in two bands. As the split is small for **Zn-8**$^{+}$, it appears only as a shoulder at 451 nm while both transitions are clearly identified for **Zn-8**$^{2+}$ at 443 and 460 nm (see also Supporting Information Figure S87).

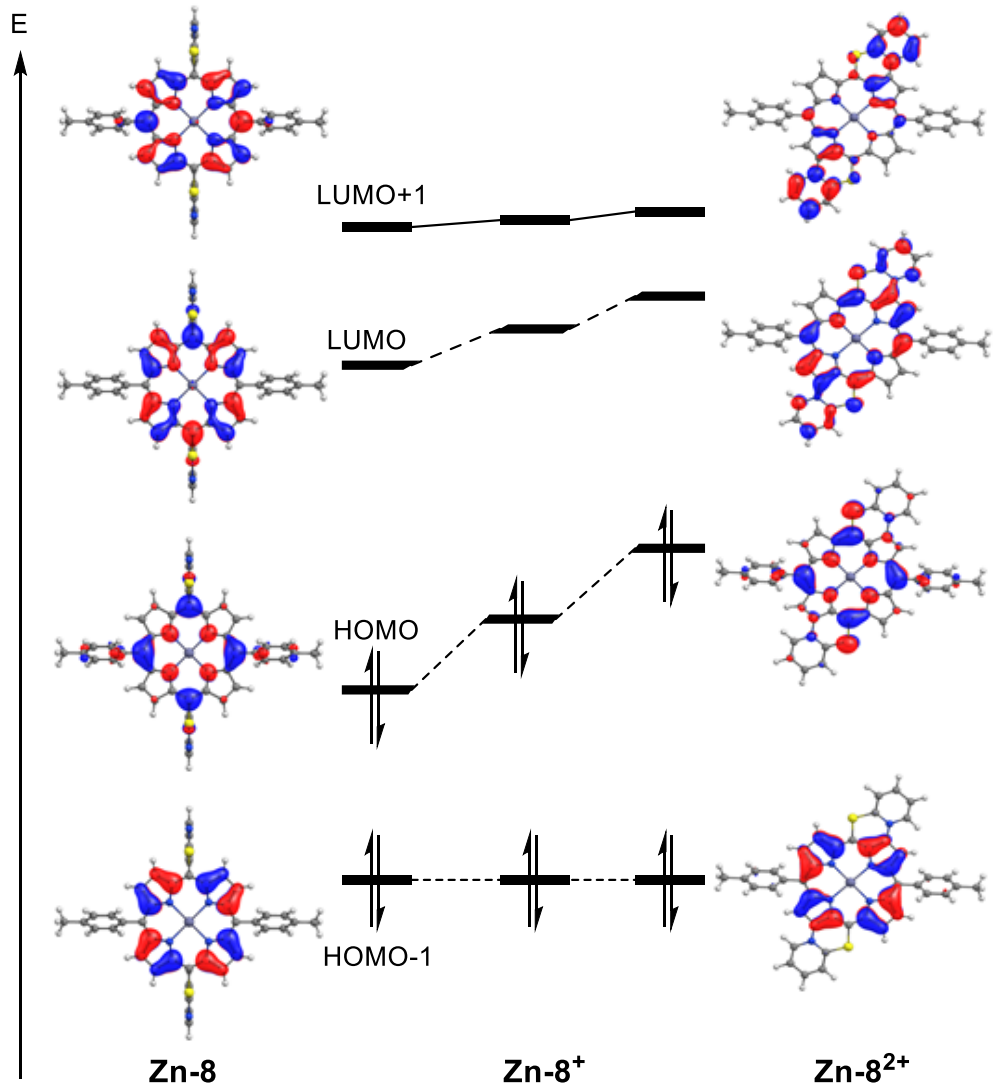

Figure 8. Schematic evolution of the energies for the four orbitals of the Gouterman model along the C-N fusions.

As an ultimate proof of the molecular structure of the C-N fused derivatives, the X-ray crystallographic structures of **Zn-6$^+$,PF$_6^-$** and **Zn-8$^+$,PF$_6^-$** were solved by analyzing suitable monocrystals grown by slow diffusion of Et_2O or MeOH, respectively, into a concentrated solution of the porphyrin in CH_2Cl_2 in the presence of two drops of pyridine (Figures 9 and S85 for **Zn-6$^+$,PF$_6^-$** and Figures 10 and S86 for **Zn-8$^+$,PF$_6^-$**). For both porphyrins, the C-N fused thiopyridinyl unit is coplanar with the porphyrin ring and the positive charge of the cationic fused porphyrins is confirmed by the presence of the PF_6^- anion. In the specific case of **Zn-6$^+$,PF$_6^-$**, two slightly structurally different porphyrins (porphyrin 1 and porphyrin 2) are coordinated by one pyridine axial ligand (only porphyrin 2 is shown in Figure 9). Moreover, one CH_2Cl_2 and one non-coordinated pyridine molecules are observed in the asymmetric unit. **Zn-8$^+$,PF$_6^-$** crystallizes in the presence of one CH_2Cl_2 and one MeOH molecules and the zinc(II) cation is also axially coordinated by one pyridine ligand. For **Zn-6$^+$,PF$_6^-$** and **Zn-8$^+$,PF$_6^-$**, the newly formed C-N bonds measure 1.425(6) (porphyrin 1), 1.423(6) (porphyrin 2) and 1.420(3) Å that are shorter than other unfused C_{meso}-$N_{pyridinium}$ porphyrins ($1.458 \leq d(C_{meso}\text{-}N_{pyridinium}) \leq 1.500$ Å).[97,98,32] The C_{meso}-S distance(s) are 1.764(5) (porphyrin 1), 1.763(5) (porphyrin 2) and 1.756(2) Å. The C_{meso}-S-$C_{pyridine}$ angles measure 106.5(2) (porphyrin 1), 106.3(2) (porphyrin 2) and 106.28(10)°, respectively. These values are higher by *ca*. 3° as compared to the unfused porphyrins accounting for the high

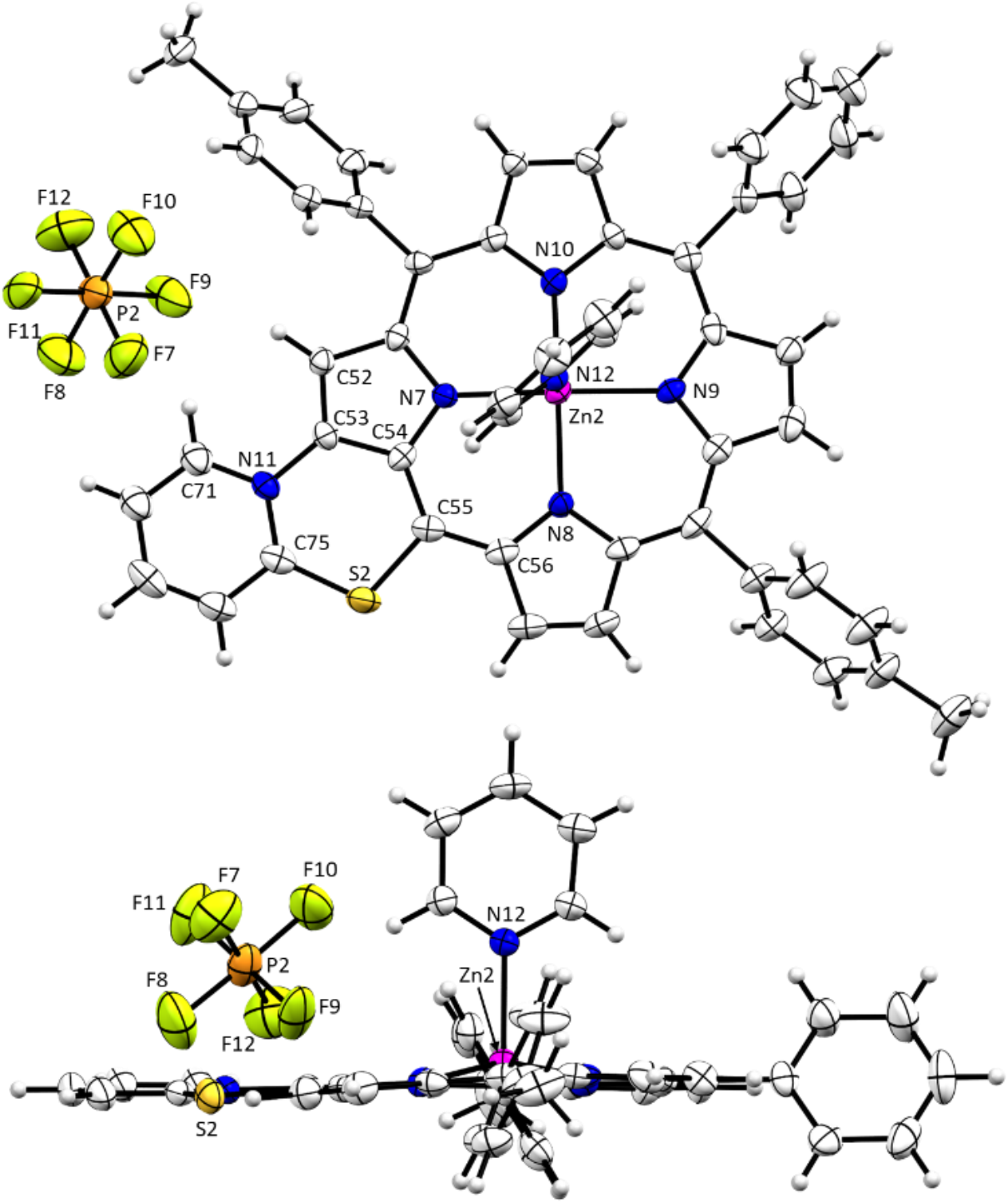

Figure 9. Front (top) and side (bottom) Mercury[90] views of **Zn-6^{+},PF$_6^{-}$•pyridine**. Thermal ellipsoids are scaled to the 50% probability level. Solvents and porphyrin 1 were removed for clarity.

flexibility of the sulfur atom. In agreement with the planar structure of the C-N fused porphyrins, the torsion angles C_{porph}-C_{meso}-S-$C_{pyridinium}$ are respectively equal to 178.0(4) (porphyrin 1), −179.1(3) (porphyrin 2) and 175.46(15)°. The C_{porph}-C_{meso}-S-$C_{pyridine}$ torsion angle for the unfused thiopyridinyl fragment of **Zn-8$^+$,PF$_6^-$** is nearly orthogonal (−91.27(18)°) as already observed on the X-ray crystallographic structures of the unfused derivatives **Zn-7** and **Zn-8**.The distance between the zinc(II) atom and the mean plane of the porphyrin is 0.3834(10) (porphyrin 1), 0.4028(9) (porphyrin 2) and 0.4404(5) Å, respectively whereas the distance between the metal and the nitrogen atoms from the porphyrins varies from from 2.049(4) to 2.084(3) Å for **Zn-6$^+$,PF$_6^-$** and from 2.0618(19) and 2.0952(18) for **Zn-8$^+$,PF$_6^-$**. The distances between the nitrogen atom from the axially ligated pyridine and the zinc(II) atom is *d*(Zn-$N_{pyridine}$) = 2.120(4) (porphyrin 1), 2.122(4) (porphyrin 2) and 2.1266(17) Å respectively. Interestingly, these C-N-fused cationic porphyrins form π-stacked dimers with a slipped cofacial orientation resembling the photosynthetic special pair (see Figures S85 and S86 for **Zn-6$^+$,PF$_6^-$** and **Zn-8$^+$,PF$_6^-$**, respectively).[99] For **Zn-6$^+$,PF$_6^-$**, the shortest interplanar $C_{porphyrin(1)}$-$C_{porphyrin(2)}$ distances are 3.260(8), 3.344(7), 3.350(7) and 3.369(7) Å while for **Zn-8$^+$,PF$_6^-$**, these distances are equal to 3.317(3), 3.329(3), 3.337(3) and 3.340(3) Å. In this case, the two porphyrin planes are parallel. Thus the distance between the mean planes formed by the 24 C and N atoms of each porphyrin ring measures 3.296(4) Å whereas the centroid-centroid distance between parallel porphyrins is equal to 6.814(6). The difference in these two distances indicates that the porphyrin rings are strongly slipped. The slip angle between the normal to the planes and the centroid-centroid vector is 28.93(5)° corresponding to a slippage distance of 5.964(7) Å.

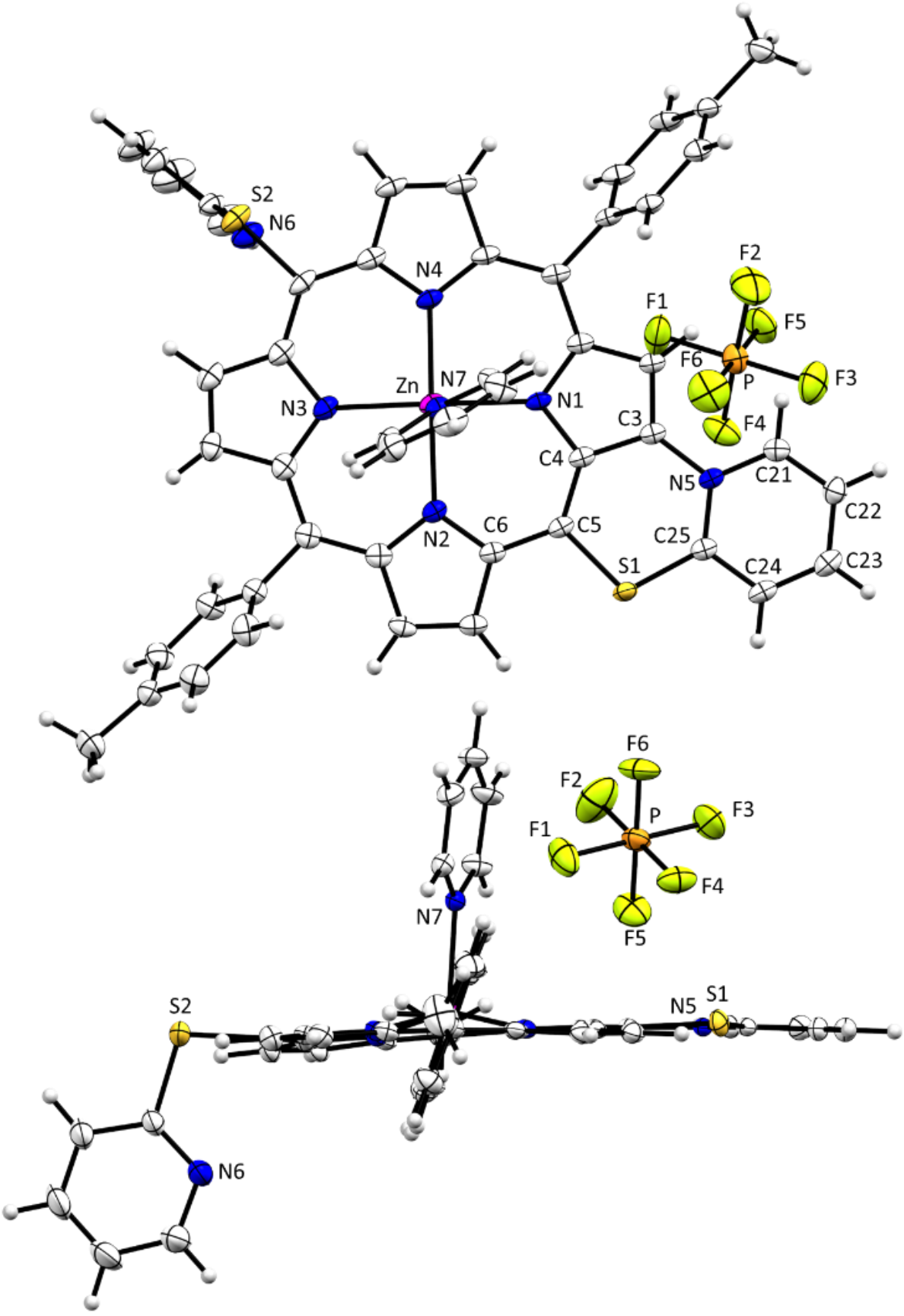
S2
N6
N4
F2
F1
F5
F6
P
F3
Zn
N7
N3
N1
C3
F4
C4
N5
C21
C22
N2
C6
C5
C25
C24
C23
S1
F6
F2
P
F3
F1
F4
F5
N7
S2
N5
S1
N6

Figure 10. Front (top) and side (bottom) Mercury[90] views of **Zn-8$^+$,PF$_6^-$•pyridine**. Thermal ellipsoids are scaled to the 50% probability level. Solvent molecules were removed for clarity.

Specific oxidative behavior of porphyrin Zn-7.

In our previous communication, the chemical or electrochemical oxidation of the nickel(II) complex analogue of **Zn-7**, **Ni-7**, only led to the C-N fused product in high yield and good selectivity (71% yield, **M-7** → **Ni-7$^+$,A$^-$** reaction in Scheme 3).[23]

Scheme 3. Oxidative behavior of **M-7** with M = Ni (previous work[23]) and M = Zn (this work).

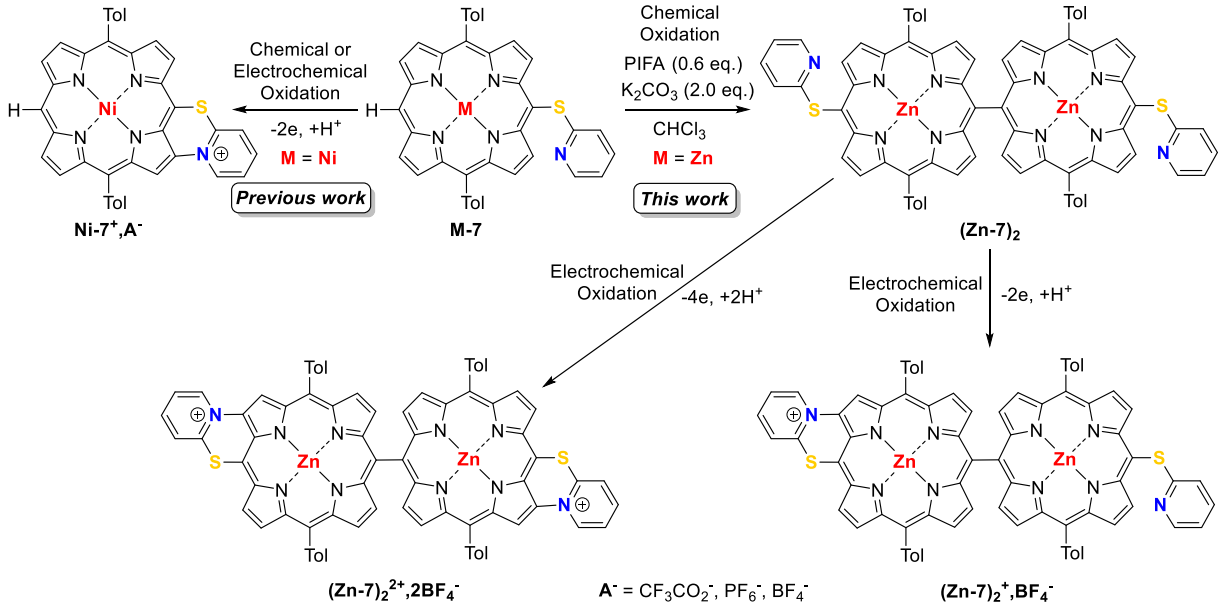

Replacing the nickel(II) metal by the zinc(II) ion in the porphyrin core totally changed the selectivity of the reaction. After optimization, the chemical oxidation of **Zn-7** in $CHCl_3$ with 0.6 eq. of PIFA[100,101] and 2 eq. of K_2CO_3 afforded the *meso,meso*-linked porphyrin dimer **(Zn-7)$_2$** as the main product (71% isolated yield, Scheme 3). No trace of the C-N fused monomer was observed but the mono-C-N fused *meso,meso*-dimer **(Zn-7)$_2^+$,CF$_3$CO$_2^-$** was systematically formed as a side-product in yields lower than 20%. This *meso,meso* regioselectivity has been previously observed when zinc(II) porphyrins bearing at least one *meso*-free position are

oxidized.[102–106,57] **(Zn-7)$_2$** showed typical *meso*,*meso*-dimer signature such as high field shift of the inner β-pyrrolic proton signals (from 8.48 ppm for **Zn-7** to 7.88 ppm for **(Zn-7)$_2$** in $(CD_3)_2SO$, see Figure 11, top) and Davydov splitting of the Soret band (from 427 nm for **Zn-7** to 432 and 468 nm for **(Zn-7)$_2$** in DMSO, Figure 12).

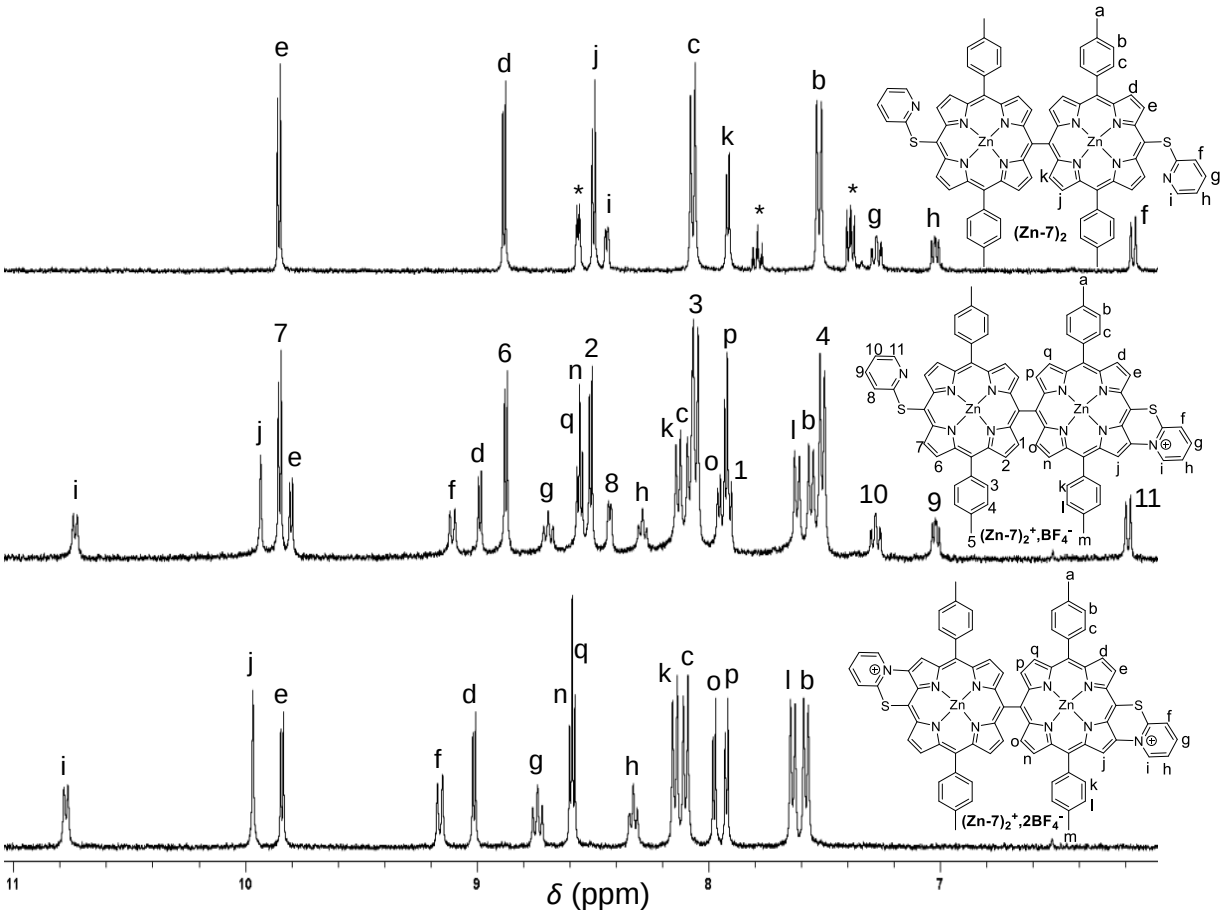

Figure 11. Partial ^{1}H NMR spectra of **(Zn-7)$_2$** (top), **(Zn-7)$_2^+$,BF$_4^-$** (middle) and **(Zn-7)$_2^{2+}$,2BF$_4^-$** (bottom). Asterisks (*) correspond to decoordinated pyridine. Conditions: $(CD_3)_2SO$, 500 MHz, 300 K.

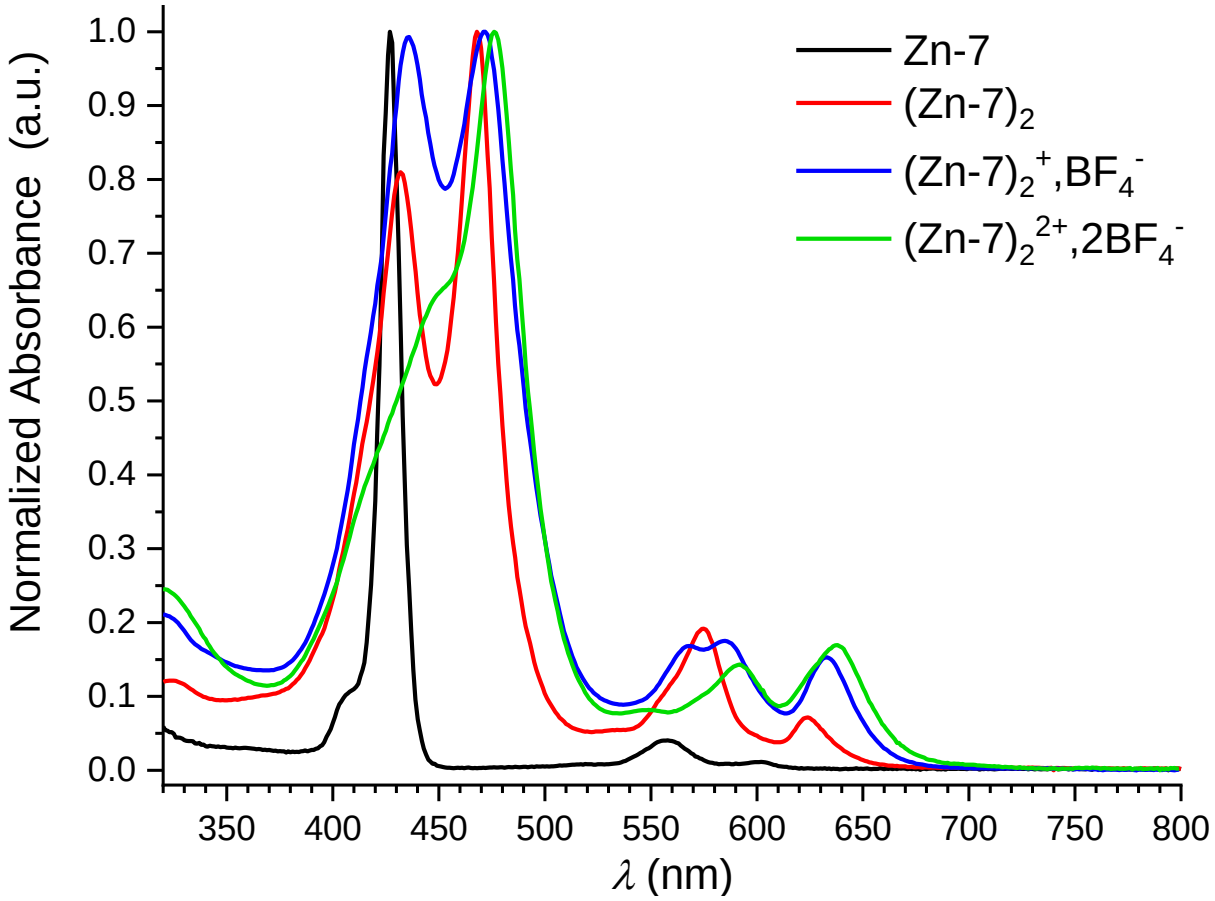

Figure 12. Normalized UV-visible absorption spectra of **Zn-7** (black curve), **(Zn-7)$_2$** (red curve), **(Zn-7)$_2^+$,BF$_4^-$** (blue curve) and **(Zn-7)$_2^{2+}$,2BF$_4^-$** (green curve) in DMSO at room temperature.

Monocrystals of **(Zn-7)$_2$** suitable for X-ray diffraction analyses were obtained by slow diffusion of MeOH in a concentrated solution of **(Zn-7)$_2$** in CH_2Cl_2 (Figure 13). According to the CCDC database, this structure is the seventh zinc(II) *meso-meso* porphyrin dimer reported to date.[107–109,81,110,57,111]

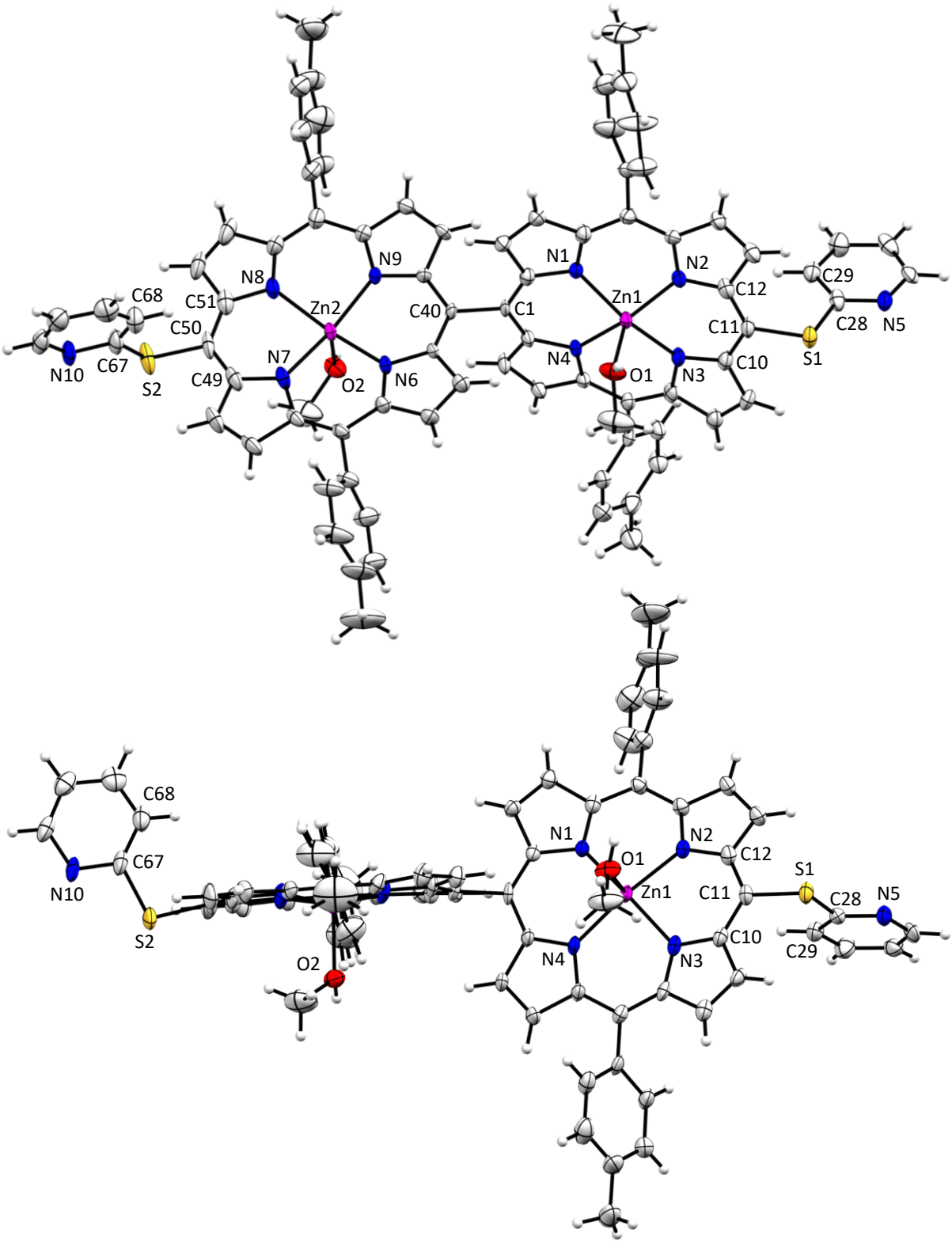
N9
N8
C68
C51
Zn2
C40
C1
N1
N2
C29
C12
C50
N7
C49
O2
N6
N4
O1
N3
C10
C11
C28
N5
S1
N10
C67
S2
C68
N1
N2
C12
O1
S1
N10
C67
Zn1
C11
C28
N5
S2
O2
N4
N3
C10
C29

Figure 13. Front (top) and side (bottom) Mercury[90] views of **(Zn-7)$_2$•2MeOH**. Thermal ellipsoids are scaled to the 50% probability level. Solvent molecules (CH_2Cl_2) were removed for clarity.

The C_{meso}-S distances, C_{meso}-S-$C_{pyridine}$ angles and torsion angles C_{porph}-C_{meso}-S-$C_{pyridine}$ are in the same range as the values found for **7**, **Zn-7** and **Zn-8** (1.774(9) and 1.782(9) Å, 103.1(5) and 104.4(5)°, -87.4(8) and 83.0(11)°, respectively for each monomer unit of the dimer). The distances between the zinc(II) atoms and the mean plane of the porphyrins are 0.275(2) and 0.309(2) Å, respectively whereas the distances between the metal and the nitrogen atoms from the porphyrins vary from 2.047(8) to 2.085(8) Å. **(Zn-7)$_2$** is coordinated by two MeOH molecules (2.087(7) < *d*(Zn-O) < 2.088(7) Å). The angle between the two porphyrin mean planes is 71.37(6)°. The *meso*,*meso* bond measures 1.515(10) Å which is close to other *meso*,*meso* distances already reported for Zn(II) *meso*,*meso*-dimer.[107–109,81,110,57,111]

The CV of **(Zn-7)$_2$** was studied in CH_2Cl_2 (0.1 M $TBAPF_6$) in the presence of 1 eq. of pyridine (Figure 14, top). The voltammogram showed various redox systems. The first monoelectronic oxidation peak (E_{pa}(O1) = 0.91 V) is only slightly reversible. The second oxidation peak O2 (E_{pa}(O2) = 1.17 V) is very broad since it covers several oxidative transformations. In the negative potential direction, only two reversible mono-electronic reductions are observed at $E_{1/2}$ = −1.17 and −1.29 V (R1 and R2 redox systems). They are attributed to the successive formation of the mono(anion radical) then bis(anion radical) of the porphyrin dimer.[57,112] Given the small potential gap between the first and second oxidation peaks as well as the decrease of the oxidative power of PIFA in the presence of pyridine, we only considered the electrochemical method to reach a better selectivity for the next oxidative transformations. The oxidation of **(Zn-7)$_2$** dimer at E_{app} = 0.92 V (−2.0 F/mol *vs* **(Zn-7)$_2$**) mainly produces the mono-C-N fused

derivative **(Zn-7)$_2^+$,BF$_4^-$** which was isolated in 57% yield. When a higher charge was applied during the electrolysis (−4.8 F/mol *vs* **(Zn-7)$_2$**), the doubly C-N fused dimer **(Zn-7)$_2^{2+}$,2BF$_4^-$** was synthesized in 98% isolated yield. Noteworthy, β,β-triply-fused porphyrin dimer was not detected in the crude mixture of these two experiments, in agreement with the CV analyses.

The NMR analyses confirm the molecular structure of the C-N fused compounds **(Zn-7)$_2^+$,BF$_4^-$** and **(Zn-7)$_2^{2+}$,2BF$_4^-$** (Figure 11, middle and bottom, respectively and ESI for complete NMR characterization). Specifically for **(Zn-7)$_2^+$,BF$_4^-$**, the unfused pyridinyl proton signals (H11, H9, H10, H8, see the attribution on the molecular structure of **(Zn-7)$_2^+$,BF$_4^-$** drawn on the middle spectrum of Figure 11) appear at 6.18, 7.02, 7.28 and 8.44 ppm, respectively. The chemical shifts of these signals are very close to the one observed for the non-fused dimer **(Zn-7)$_2$** (Hf, Hh, Hg and Hi at 6.15, 7.01, 7.27 and 8.44 ppm, respectively, see the attribution on the top of Figure 11) highlighting the very weak influence of the neighboring C-N fused porphyrin. The same feature is also observed for the other signals of the non-fused porphyrin unit (β-pyrrolic and tolyl protons) since they are observed at very similar chemical shifts than **(Zn-7)$_2$**. On the other hand, the pyridinium proton signals of the C-N fused porphyrin moiety (Hh, Hg, Hf, Hi) appear at much lower field (8.27, 8.67, 9.08 and 10.72 ppm, respectively), as mentioned earlier for the C-N fused porphyrin monomers **Zn-6$^+$,PF$_6^-$**, **Zn-8$^+$,PF$_6^-$** and **Zn-8^{2+},2BF$_4^-$**. The doubly C-N fused dimer **(Zn-7)$_2^{2+}$,2BF$_4^-$** also exhibits highly unshielded pyridinium signals (Hh, Hg, Hf and Hi) that appear at 8.26, 8.66, 9.05 and 10.72 ppm, respectively, values that are also very close to the one observed for the C-N fused porphyrin unit of **(Zn-7)$_2^+$,BF$_4^-$**. Another characteristic feature of these C-N fused porphyrin concerns the presence of one β-pyrrolic singlet (Hj) which integrates for one proton for **(Zn-7)$_2^+$,BF$_4^-$** and two protons for **(Zn-7)$_2^{2+}$,2BF$_4^-$**. Besides, contrary to **(Zn-7)$_2^+$,BF$_4^-$** for which three methyl singlets are observed at

2.56 (H5, 2H), 2.59 (Ha, 1H) and 2.63 ppm (Hm, 1H), **(Zn-7)$_2^{2+}$,2BF$_4^-$** exhibits only two methyl singlets at 2.60 (Ha, 2H) and 2.64 ppm (Hm, 2H) due to its highest symmetry.

The CVs of **(Zn-7)$_2^+$,BF$_4^-$** and **(Zn-7)$_2^{2+}$,2BF$_4^-$** are shown in Figure 14 (middle and bottom CVs, respectively).

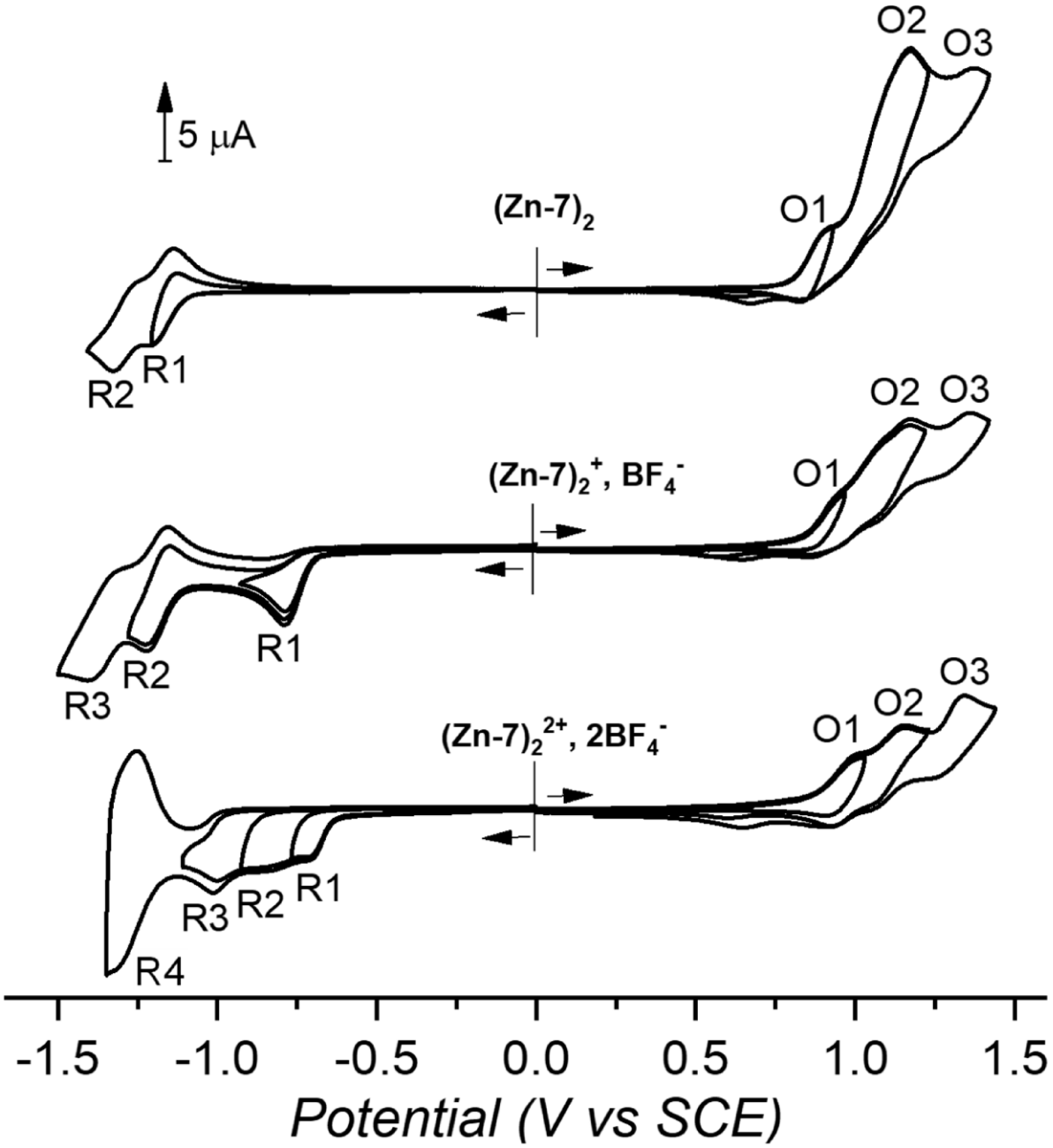

Figure 14. Cyclic voltammograms of **(Zn-7)$_2$**, **(Zn-7)$_2^+$,BF$_4^-$** and **(Zn-7)$_2^{2+}$,2BF$_4^-$** (CH_2Cl_2/CH_3CN (4:1 v/v) 0.1 M $TEABF_4$ + 1.0 equiv. (for **(Zn-7)$_2$** and **(Zn-7)$_2^+$,BF$_4^-$**) or 2 eq. (for **(Zn-7)$_2^{2+}$,2BF$_4^-$**) of pyridine, $c = 10^{-3}$ M, $v = 100$ mV s^{-1}, WE: Pt, $\varnothing = 1.6$ mm).

One pyridinium-centered irreversible reduction (R1 peak, E_{pc}(R1) = −0.79 V) is observed for **(Zn-7)$_2^+$,BF$_4^-$** whereas two pyridinium-centered irreversible reductions (R1 and R2 peaks, E_{pc}(R1) = −0.71 V, E_{pc}(R2) ≈ −0.86 V) are seen for **(Zn-7)$_2^{2+}$,2BF$_4^-$**, in agreement with their respective molecular structures. Two reversible monoelectronic oxidation peaks ($E_{1/2}$(O1) = 0.96 and $E_{1/2}$(O2) = 1.10 V) are observed for **(Zn-7)$_2^{2+}$,2BF$_4^-$**. The potential gap between these macrocycle-centered oxidations (monoelectronic oxidation of one porphyrin ring then monoelectronic oxidation of the other porphyrin ring) corresponds to 140 mV, in agreement with other *meso*,*meso*-linked porphyrin dimers.[104,113,82,112,57] The UV-visible absorption spectra of **Zn-7**, **(Zn-7)$_2$**, **(Zn-7)$_2^+$,BF$_4^-$** and **(Zn-7)$_2^{2+}$,2BF$_4^-$** are gathered in Figure 12. Going from **(Zn-7)$_2$** to **(Zn-7)$_2^+$,BF$_4^-$** to **(Zn-7)$_2^{2+}$,2BF$_4^-$**, the highest energy Soret band undergoes a progressive bathochromic shift from 432 nm for **(Zn-7)$_2$** to 435 nm for **(Zn-7)$_2^+$,BF$_4^-$** (non-measurable broad band for **(Zn-7)$_2^{2+}$,2BF$_4^-$**). Similar behavior was also observed for the lowest energy Soret band which absorption maximum spans from 468 to 472 to 476 nm, respectively. The Q bands also experience a progressive bathochromic shift. For example, the lowest energy Q band goes from 624 to 633 to 638 nm, respectively.

In the dimer, the interactions between the two moieties lead to the splitting of the four Gouterman's orbitals into eight orbitals in the dimers (see Figure S89 in SI). This gives rise to four possible transitions for the Q and B bands. However, as the orbital splitting are uneven, the transitions cannot be fully resolved and appear as two B bands and two Q bands for **(Zn-7)$_2$**. The

C-N fusion increases the π-conjugation so that the bands are shifted toward higher wavelengths from **(Zn-7)$_2$** to **(Zn-7)$_2^+$** and **(Zn-7)$_2^{2+}$**.

CONCLUSION

Three original zinc(II) *meso*-pyridin-2-ylthio-porphyrins (**Zn-6**, **Zn-7**, **Zn-8**) have been prepared and characterized by NMR, UV-vis., CV, MS and for **Zn-7** and **Zn-8**, by X-ray diffraction analyses. The **Zn-8** crystallographic structure reveals a very rare coordination trimer. In the case of fully *meso*-substituted porphyrins (**Zn-6** and **Zn-8**), the chemical and electrochemical oxidations of the porphyrin ring induce an intramolecular C-N fusion of the pyridinyl peripheral substituent affording the cationic and planar **Zn-6$^+$,PF$_6^-$** and **Zn-8$^+$,PF$_6^-$** whose structures were solved by X-ray diffraction analyses. While the chemical oxidation of the 5,15-doubly-substituted-pyridinyl porphyrin **Zn-8** with PIFA excess produces sulfone and sulfoxides, the electrochemical oxidation was proved to be more selective as oxidation of **Zn-8** at its second oxidation potential provides the doubly C-N fused dicationic derivative. Upon oxidation, the **Zn-7** unfused precursor, which bears one *meso*-free position, first dimerizes into the *meso*,*meso*-dimer (**Zn-7)$_2$** which was characterized by X-ray diffraction. Further oxidation produces consecutively the mono C-N fused **(Zn-7)$_2^+$,BF$_4^-$** and then the doubly C-N fused **(Zn-7)$_2^{2+}$,2BF$_4^-$** *meso*,*meso*-dimers. Due to the planarization of the molecules and to the positive charges that are formed, the C-N fusion reaction induces important electronic changes that are revealed on the UV-vis absorption spectra (bathochromic shift of the Soret and Q bands, splitting of the Soret bands) and on the cyclic voltammograms (reduction of the pyridinium moity(ies) between −0.5 and −1.0 V). The chemical reactivity and possible applications of the C-N fused porphyrins are now under investigation.

ASSOCIATED CONTENT

Supporting Information. The Supporting Information is available free of charge at https://pubs.acs.org/. Additional experimental details and experimental procedures for the preparation of porphyrins, NMR spectra, HRMS spectra, UV-visible absorption spectra, cyclic voltammograms for all compounds, crystallographic data for **7**, **Zn-7**, **Zn-8**, **(Zn-7)$_2$**, **Zn-6$^+$,PF$_6^-$**, **Zn-8$^+$,PF$_6^-$** and DFT TD/DFT calculations.

AUTHOR INFORMATION

Corresponding Author

Charles H. Devillers - Institut de Chimie Moléculaire de l'Université de Bourgogne (ICMUB), UMR6302, CNRS, Univ. Bourgogne Franche-Comté, 9 avenue Alain Savary, 21000 Dijon, France ; E-mail: charles.devillers@u-bourgogne.fr

Authors

Mathieu Berthelot - Institut de Chimie Moléculaire de l'Université de Bourgogne, UMR6302, CNRS, Univ. Bourgogne Franche-Comté, 9 avenue Alain Savary, 21000 Dijon, France

Fatima Akhssas - Institut de Chimie Moléculaire de l'Université de Bourgogne, UMR6302, CNRS, Univ. Bourgogne Franche-Comté, 9 avenue Alain Savary, 21000 Dijon, France

Abdou K. D. Dimé - Département de Chimie, UFR SATIC, Université Alioune Diop de Bambey, Senegal

Asmae Bousfiha - Institut de Chimie Moléculaire de l'Université de Bourgogne, UMR6302, CNRS, Univ. Bourgogne Franche-Comté, 9 avenue Alain Savary, 21000 Dijon, France

Julie Echaubard - Institut de Chimie Moléculaire de l'Université de Bourgogne, UMR6302, CNRS, Univ. Bourgogne Franche-Comté, 9 avenue Alain Savary, 21000 Dijon, France

Ghada Souissi - Institut de Chimie Moléculaire de l'Université de Bourgogne, UMR6302, CNRS, Univ. Bourgogne Franche-Comté, 9 avenue Alain Savary, 21000 Dijon, France

Hélène Cattey - Institut de Chimie Moléculaire de l'Université de Bourgogne, UMR6302, CNRS, Univ. Bourgogne Franche-Comté, 9 avenue Alain Savary, 21000 Dijon, France

Dominique Lucas - Institut de Chimie Moléculaire de l'Université de Bourgogne, UMR6302, CNRS, Univ. Bourgogne Franche-Comté, 9 avenue Alain Savary, 21000 Dijon, France

Paul Fleurat-Lessard - Institut de Chimie Moléculaire de l'Université de Bourgogne, UMR6302, CNRS, Univ. Bourgogne Franche-Comté, 9 avenue Alain Savary, 21000 Dijon, France

Author Contributions

‡ M. B. and F. A. contributed equally to this work. The manuscript was written through contributions of all authors. All authors have given approval to the final version of the manuscript.

ACKNOWLEDGMENT

This work was supported by the Université de Bourgogne Franche-Comté, CNRS (Centre National de la Recherche Scientifique), Conseil Régional de Bourgogne through the "Plan d'Actions Régional pour l'Innovation (PARI)" and the "Fonds Européen de Développement Régional (FEDER)" programs). M.B., A.B., G.S. and C.H.D. thank the Agence Nationale de la Recherche for funding (ANR-15-CE28-0018-01). F.A. and C.H.D. acknowledge the Conseil Régional de Bourgogne Franche-Comté for a PhD grant (PORFELEC project) and the French "Investissement d'Avenir" program, project ISITE-BFC (contract ANR-15-IDEX-03) for funding. A.B. acknowledges the Ministère de l'Enseignement Supérieur, de la Recherche et de l'Innovation for a PhD grant. The authors are thankful to Sophie Fournier for technical support,

to Dr. David Monchaud and Marc Pirotta for fluorescence measurements and to the ‘‘Plateforme d’Analyse Chimique et de Synthèse Moléculaire de l’Université de Bourgogne” (PACSMUB, http://www.wpcm.fr) for ESI-HRMS analyses. This work was granted access to the HPC resources of 1) CINES under the allocation A0090807259 made by GENCI and 2) DSI-CCUB (Université de Bourgogne).

REFERENCES

(1) Grzybowski, M.; Skonieczny, K.; Butenschön, H.; Gryko, D. T. Comparison of Oxidative Aromatic Coupling and the Scholl Reaction. *Angew. Chem., Int. Ed.* **2013**, *52* (38), 9900–9930. https://doi.org/10.1002/anie.201210238.

(2) Matsuo, Y.; Sato, Y.; Niinomi, T.; Soga, I.; Tanaka, H.; Nakamura, E. Columnar Structure in Bulk Heterojunction in Solution-Processable Three-Layered p-i-n Organic Photovoltaic Devices Using Tetrabenzoporphyrin Precursor and Silylmethyl[60]Fullerene. *J. Am. Chem. Soc.* **2009**, *131* (44), 16048–16050. https://doi.org/10.1021/ja9048702.

(3) Zimmerman, J. D.; Diev, V. V.; Hanson, K.; Lunt, R. R.; Yu, E. K.; Thompson, M. E.; Forrest, S. R. Porphyrin-Tape/C60 Organic Photodetectors with 6.5% External Quantum Efficiency in the Near Infrared. *Adv. Mater.* **2010**, *22* (25), 2780–2783. https://doi.org/10.1002/adma.200904341.

(4) Jurow, M.; Schuckman, A. E.; Batteas, J. D.; Drain, C. M. Porphyrins as Molecular Electronic Components of Functional Devices. *Coord. Chem. Rev.* **2010**, *254* (19), 2297–2310. https://doi.org/10.1016/j.ccr.2010.05.014.

(5) Satrialdi; Munechika, R.; Biju, V.; Takano, Y.; Harashima, H.; Yamada, Y. The Optimization of Cancer Photodynamic Therapy by Utilization of a Pi-Extended Porphyrin-Type

Photosensitizer in Combination with MITO-Porter. *Chem. Commun.* **2020**, *56* (7), 1145–1148. https://doi.org/10.1039/C9CC08563G.

(6) Rath, H.; Sankar, J.; PrabhuRaja, V.; Chandrashekar, T. K.; Nag, A.; Goswami, D. Core-Modified Expanded Porphyrins with Large Third-Order Nonlinear Optical Response. *J. Am. Chem. Soc.* **2005**, *127* (33), 11608–11609. https://doi.org/10.1021/ja0537575.

(7) Fenwick, O.; Sprafke, J. K.; Binas, J.; Kondratuk, D. V.; Di Stasio, F.; Anderson, H. L.; Cacialli, F. Linear and Cyclic Porphyrin Hexamers as Near-Infrared Emitters in Organic Light-Emitting Diodes. *Nano Lett.* **2011**, *11* (6), 2451–2456. https://doi.org/10.1021/nl2008778.

(8) Saegusa, Y.; Ishizuka, T.; Komamura, K.; Shimizu, S.; Kotani, H.; Kobayashi, N.; Kojima, T. Ring-Fused Porphyrins: Extension of π-Conjugation Significantly Affects the Aromaticity and Optical Properties of the Porphyrin π-Systems and the Lewis Acidity of the Central Metal Ions. *Phys. Chem. Chem. Phys.* **2015**, *17* (22), 15001–15011. https://doi.org/10.1039/C5CP01420D.

(9) Sahoo, A. K.; Mori, S.; Shinokubo, H.; Osuka, A. Facile Peripheral Functionalization of Porphyrins by Pd-Catalyzed [3+2] Annulation with Alkynes. *Angew. Chem., Int. Ed.* **2006**, *45*, 7972–7975. https://doi.org/10.1002/anie.200603580.

(10) Shen, D.-M.; Liu, C.; Chen, Q.-Y. A General and Efficient Palladium-Catalyzed Intramolecular Cyclization Reaction of β-Brominated Porphyrins. *J. Org. Chem.* **2006**, *71*, 6508–6511. https://doi.org/10.1021/jo0609677.

(11) Tanaka, T.; Osuka, A. Triply Linked Porphyrinoids. *Chem. − Eur. J.* **2018**, *24* (65), 17188–17200. https://doi.org/10.1002/chem.201802810.

(12) Nowak-Król, A.; Gryko, D. T. Oxidative Aromatic Coupling of Meso-Arylamino-Porphyrins. *Org. Lett.* **2013**, *15* (22), 5618–5621. https://doi.org/10.1021/ol4022035.

(13) Bengasi, G.; Baba, K.; Frache, G.; Desport, J.; Gratia, P.; Heinze, K.; Boscher, N. D. Conductive Fused Porphyrin Tapes on Sensitive Substrates by a Chemical Vapor Deposition Approach. *Angew. Chem., Int. Ed.* **2019**, *58* (7), 2103–2108. https://doi.org/10.1002/anie.201814034.

(14) Davis, N. K. S.; Pawlicki, M.; Anderson, H. L. Expanding the Porphyrin π-System by Fusion with Anthracene. *Org. Lett.* **2008**, *10* (18), 3945–3947. https://doi.org/10.1021/ol801500b.

(15) Bengasi, G.; Baba, K.; Back, O.; Frache, G.; Heinze, K.; Boscher, N. D. Reactivity of Nickel(II) Porphyrins in OCVD Processes—Polymerisation, Intramolecular Cyclisation and Chlorination. *Chem. – Eur. J.* **2019**, *25* (35), 8313–8320. https://doi.org/10.1002/chem.201900793.

(16) Yamashita, K.; Hirano, D.; Fujimaki, K.; Sugiura, K. Synthesis of Porphyrinquinone and Doubly-Fused Diporphyrin Quinone Through Oxidation of Diarylporphyrins Using a Hypervalent Iodine Compound. *Chem. Asian J.* **2020**, *15* (19), 3037–3043. https://doi.org/10.1002/asia.202000781.

(17) Richeter, S.; Jeandon, C.; Gisselbrecht, J.-P.; Graff, R.; Ruppert, R.; Callot, H. J. Synthesis of New Porphyrins with Peripheral Conjugated Chelates and Their Use for the Preparation of Porphyrin Dimers Linked by Metal Ions. *Inorg. Chem.* **2004**, *43* (1), 251–263. https://doi.org/10.1021/ic035203d.

(18) Diev, V. V.; Schlenker, C. W.; Hanson, K.; Zhong, Q.; Zimmerman, J. D.; Forrest, S. R.; Thompson, M. E. Porphyrins Fused with Unactivated Polycyclic Aromatic Hydrocarbons. *J. Org. Chem.* **2012**, *77* (1), 143–159. https://doi.org/10.1021/jo201490y.

(19) Pereira, A. M. V. M.; Alonso, C. M. A.; Neves, M. G. P. M. S.; Tomé, A. C.; Silva, A. M. S.; Paz, F. A. A.; Cavaleiro, J. A. S. A New Synthetic Approach to N-Arylquinolino[2,3,4-at]Porphyrins from β-Arylaminoporphyrins. *J. Org. Chem.* **2008**, *73* (18), 7353–7356. https://doi.org/10.1021/jo800975c.

(20) Thuita, D.; Guberman-Pfeffer, M. J.; Brückner, C. SNAr Reaction Toward the Synthesis of Fluorinated Quinolino[2,3,4-at]Porphyrins. *Eur. J. Org. Chem.* **2021**, *2021* (2), 318–323. https://doi.org/10.1002/ejoc.202001347.

(21) Chen, P.; Fang, Y.; Kadish, K. M.; Lewtak, J. P.; Koszelewski, D.; Janiga, A.; Gryko, D. T. Electrochemically Driven Intramolecular Oxidative Aromatic Coupling as a Pathway toward π-Extended Porphyrins. *Inorg. Chem.* **2013**, *52* (16), 9532–9538. https://doi.org/10.1021/ic401214e.

(22) Fang, Y.; Koszelewski, D.; Kadish, K. M.; Gryko, D. T. Facile Electrosynthesis of π-Extended Porphyrins. *Chem. Commun.* **2014**, *50* (64), 8864–8867. https://doi.org/10.1039/C4CC02759K.

(23) Berthelot, M.; Hoffmann, G.; Bousfiha, A.; Echaubard, J.; Roger, J.; Cattey, H.; Romieu, A.; Lucas, D.; Fleurat-Lessard, P.; Devillers, C. H. Oxidative C-N Fusion of Pyridinyl-Substituted Porphyrins. *Chem. Commun.* **2018**, *54* (43), 5414–5417. https://doi.org/10.1039/C8CC01375F.

(24) Smith, K. M.; Barnett, G. H.; Evans, B.; Martynenko, Z. Novel Meso-Substitution Reactions of Metalloporphyrins. *J. Am. Chem. Soc.* **1979**, *101* (20), 5953–5961. https://doi.org/10.1021/ja00514a015.

(25) Giraudeau, A.; Ruhlmann, L.; El Kahef, L.; Gross, M. Electrosynthesis and Characterization of Symmetrical and Unsymmetrical Linear Porphyrin Dimers and Their Precursor Monomers. *J. Am. Chem. Soc.* **1996**, *118* (12), 2969–2979. https://doi.org/10.1021/ja9523956.

(26) Ruhlmann, L.; Schulz, A.; Giraudeau, A.; Messerschmidt, C.; Fuhrhop, J.-H. A Polycationic Zinc-5,15-Dichlorooctaethylporphyrinate-Viologen Wire. *J. Am. Chem. Soc.* **1999**, *121* (28), 6664–6667. https://doi.org/10.1021/ja984404r.

(27) Schaming, D.; Ahmed, I.; Hao, J.; Alain-Rizzo, V.; Farha, R.; Goldmann, M.; Xu, H.; Giraudeau, A.; Audebert, P.; Ruhlmann, L. Easy Methods for the Electropolymerization of Porphyrins Based on the Oxidation of the Macrocycles. *Electrochim. Acta* **2011**, *56* (28), 10454–10463. https://doi.org/10.1016/j.electacta.2011.02.064.

(28) Devillers, C. H.; Dimé, A. K. D.; Cattey, H.; Lucas, D. Electrochemical Meso-Functionalization of Magnesium(II) Porphine. *Chem. Commun.* **2011**, *47* (6), 1893–1895. https://doi.org/10.1039/c0cc04309e.

(29) Xia, Y.; Schaming, D.; Farha, R.; Goldmann, M.; Ruhlmann, L. Bis-Porphyrin Copolymers Covalently Linked by Pyridinium Spacers Obtained by Electropolymerization from β-Octaethylporphyrins and Pyridyl-Substituted Porphyrins. *New J. Chem.* **2012**, *36* (3), 588–596. https://doi.org/10.1039/C1NJ20790C.

(30) Schaming, D.; Xia, Y.; Thouvenot, R.; Ruhlmann, L. An Original Electrochemical Pathway for the Synthesis of Porphyrin Oligomers. *Chem. − Eur. J.* **2013**, *19*, 1712–1719. https://doi.org/10.1002/chem.201203271.

(31) Lamare, R.; Ruhlmann, L.; Ruppert, R.; Weiss, J. Case Studies of the Radical Cation Reactivity in Meso-Aryl and Octaethyl Porphyrins. *J. Porphyrins Phthalocyanines* **2019**, *24*, 860–868. https://doi.org/10.1142/S1088424619501980.

(32) Bousfiha, A.; Dimé, A. K. D.; Mankou-Makaya, A.; Echaubard, J.; Berthelot, M.; Cattey, H.; Romieu, A.; Roger, J.; Devillers, C. H. Regioselective C–H Amination of Free Base Porphyrins via Electrogenerated Pyridinium-Porphyrins and Stabilization of Easily Oxidized Amino-Porphyrins by Protonation. *Chem. Commun.* **2020**, *56* (6), 884–887. https://doi.org/10.1039/C9CC07351E.

(33) Yi, H.; Tang, Z.; Bian, C.; Chen, H.; Qi, X.; Yue, X.; Lan, Y.; Lee, J.-F.; Lei, A. Oxidation-Induced C–H Amination Leads to a New Avenue to Build C–N Bonds. *Chem. Commun.* **2017**, *53* (64), 8984–8987. https://doi.org/10.1039/C7CC04955B.

(34) Yan, M.; Kawamata, Y.; Baran, P. S. Synthetic Organic Electrochemical Methods Since 2000: On the Verge of a Renaissance. *Chem. Rev.* **2017**, *117* (21), 13230–13319. https://doi.org/10.1021/acs.chemrev.7b00397.

(35) Kärkäs, M. D. Electrochemical Strategies for C–H Functionalization and C–N Bond Formation. *Chem. Soc. Rev.* **2018**, *47* (15), 5786–5865. https://doi.org/10.1039/C7CS00619E.

(36) Yu, Y.; Yuan, Y.; Liu, H.; He, M.; Yang, M.; Liu, P.; Yu, B.; Dong, X.; Lei, A. Electrochemical Oxidative C–H/N–H Cross-Coupling for C–N Bond Formation with Hydrogen Evolution. *Chem. Commun.* **2019**, *55* (12), 1809–1812. https://doi.org/10.1039/C8CC09899A.

(37) Waldvogel, S. R.; Lips, S.; Selt, M.; Riehl, B.; Kampf, C. J. Electrochemical Arylation Reaction. *Chem. Rev.* **2018**, *118* (14), 6706–6765. https://doi.org/10.1021/acs.chemrev.8b00233.

(38) Popp, G. Nucleophilic Substitutions Initiated by Electrochemical Oxidation. I. Intramolecular Nucleophilic Substitutions. *J. Org. Chem.* **1972**, *37* (20), 3058–3062. https://doi.org/10.1021/jo00985a003.

(39) Morofuji, T.; Shimizu, A.; Yoshida, J. Electrochemical Intramolecular C-H Amination: Synthesis of Benzoxazoles and Benzothiazoles. *Chem. − Eur. J.* **2015**, *21* (8), 3211–3214. https://doi.org/10.1002/chem.201406398.

(40) Saito, M.; Nishibayashi, Y.; Uemura, S. Synthesis of Dinuclear Complexes Bearing Metalloporphyrin−Phosphine Hybrid Ligands and Their Catalytic Activity toward Hydrosilylation of Ketones. *Organometallics* **2004**, *23* (17), 4012–4017. https://doi.org/10.1021/om0498201.

(41) Suijkerbuijk, B. M. J. M.; Klein Gebbink, R. J. M. Merging Porphyrins with Organometallics: Synthesis and Applications. *Angew. Chem. Int. Ed.* **2008**, *47* (39), 7396–7421. https://doi.org/10.1002/anie.200703362.

(42) Lee, C. H.; Dogutan, D. K.; Nocera, D. G. Hydrogen Generation by Hangman Metalloporphyrins. *J. Am. Chem. Soc.* **2011**, *133* (23), 8775–8777. https://doi.org/10.1021/ja202136y.

(43) Costentin Cyrille; Drouet Samuel; Robert Marc; Savéant Jean-Michel. A Local Proton Source Enhances CO2 Electroreduction to CO by a Molecular Fe Catalyst. *Science* **2012**, *338* (6103), 90–94. https://doi.org/10.1126/science.1224581.

(44) Carver, C. T.; Matson, B. D.; Mayer, J. M. Electrocatalytic Oxygen Reduction by Iron Tetra-Arylporphyrins Bearing Pendant Proton Relays. *J. Am. Chem. Soc.* **2012**, *134* (12), 5444–5447. https://doi.org/10.1021/ja211987f.

(45) Roubelakis, M. M.; Bediako, D. K.; Dogutan, D. K.; Nocera, D. G. Proton-Coupled Electron Transfer Kinetics for the Hydrogen Evolution Reaction of Hangman Porphyrins. *Energy Environ. Sci.* **2012**, *5* (7), 7737–7740. https://doi.org/10.1039/C2EE21123H.

(46) Solis, B. H.; Maher, A. G.; Honda, T.; Powers, D. C.; Nocera, D. G.; Hammes-Schiffer, S. Theoretical Analysis of Cobalt Hangman Porphyrins: Ligand Dearomatization and Mechanistic Implications for Hydrogen Evolution. *ACS Catal.* **2014**, *4* (12), 4516–4526. https://doi.org/10.1021/cs501454y.

(47) Harvey, P. D.; Tasan, S.; Gros, C. P.; Devillers, C. H.; Richard, P.; Gendre, P. L.; Bodio, E. Ruthenium and Osmium Complexes of Phosphine-Porphyrin Derivatives as Potential Bimetallic Theranostics: Photophysical Studies. *Organometallics* **2015**, *34* (7), 1218–1227. https://doi.org/10.1021/om5011808.

(48) Solis Brian H.; Maher Andrew G.; Dogutan Dilek K.; Nocera Daniel G.; Hammes-Schiffer Sharon. Nickel Phlorin Intermediate Formed by Proton-Coupled Electron Transfer in Hydrogen Evolution Mechanism. *Proc. Natl. Acad. Sci. U.S.A* **2016**, *113* (3), 485–492. https://doi.org/10.1073/pnas.1521834112.

(49) Longevial, J.-F.; Clément, S.; Wytko, J. A.; Ruppert, R.; Weiss, J.; Richeter, S. Peripherally Metalated Porphyrins with Applications in Catalysis, Molecular Electronics and Biomedicine. *Chem. – Eur. J.* **2018**, *24* (58), 15442–15460. https://doi.org/10.1002/chem.201801211.

(50) Zardi, P.; Roisnel, T.; Gramage-Doria, R. A Supramolecular Palladium Catalyst Displaying Substrate Selectivity by Remote Control. *Chem. – Eur. J.* **2019**, *25* (2), 627–634. https://doi.org/10.1002/chem.201804543.

(51) Kasemthaveechok, S.; Fabre, B.; Loget, G.; Gramage-Doria, R. Remote Ion-Pair Interactions in Fe-Porphyrin-Based Molecular Catalysts for the Hydrogen Evolution Reaction. *Catal. Sci. Technol.* **2019**, *9* (5), 1301–1308. https://doi.org/10.1039/C8CY02164C.

(52) Trouvé, J.; Zardi, P.; Al-Shehimy, S.; Roisnel, T.; Gramage-Doria, R. Enzyme-like Supramolecular Iridium Catalysis Enabling C−H Bond Borylation of Pyridines with Meta-Selectivity. *Angew. Chem., Int. Ed.* **2021**, *60* (33), 18006–18013. https://doi.org/10.1002/anie.202101997.

(53) Senge, M. O.; Feng, X. Regioselective Reaction of 5,15-Disubstituted Porphyrins with Organolithium Reagents—Synthetic Access to 5,10,15-Trisubstituted Porphyrins and Directly Meso-Meso-Linked Bisporphyrins. *J. Chem. Soc., Perkin Trans. 1* **2000**, 3615–3621. https://doi.org/10.1039/B005411I.

(54) Adler, A. D.; Longo, F. R.; Kampas, F.; Kim, J. On the Preparation of Metalloporphyrins. *J. Inorg. Nucl. Chem.* **1970**, *32*, 2443.

(55) Chen, Q.; Zhu, Y.-Z.; Fan, Q.-J.; Zhang, S.-C.; Zheng, J.-Y. Simple and Catalyst-Free Synthesis of Meso-O-, -S-, and -C-Substituted Porphyrins. *Org. Lett.* **2014**, *16* (6), 1590–1593. https://doi.org/10.1021/ol500191j.

(56) Laha, J. K.; Dhanalekshmi, S.; Taniguchi, M.; Ambroise, A.; Lindsey, J. S. A Scalable Synthesis of Meso-Substituted Dipyrromethanes. *Org. Proc. Res. Dev.* **2003**, *7* (6), 799–812. https://doi.org/10.1021/op034083q.

(57) Dimé, A. K. D.; Devillers, C. H.; Cattey, H.; Habermeyer, B.; Lucas, D. Control over the Oxidative Reactivity of Metalloporphyrins. Efficient Electrosynthesis of Meso,Meso-Linked Zinc Porphyrin Dimer. *Dalton Trans.* **2012**, *41* (3), 929–936. https://doi.org/10.1039/c1dt11330e.

(58) Collins, H. A.; Khurana, M.; Moriyama, E. H.; Mariampillai, A.; Dahlstedt, E.; Balaz, M.; Kuimova, M. K.; Drobizhev, M.; Yang, V. X. D.; Phillips, D.; Rebane, A.; Wilson, B. C.; Anderson, H. L. Blood-Vessel Closure Using Photosensitizers Engineered for Two-Photon Excitation. *Nat. Photonics* **2008**, *2*, 420–424. https://doi.org/10.1038/nphoton.2008.100.

(59) Devillers, C. H.; Hebié, S.; Lucas, D.; Cattey, H.; Clément, S.; Richeter, S. Aromatic Nucleophilic Substitution (SNAr) of Meso-Nitroporphyrin with Azide and Amines as an Alternative Metal Catalyst Free Synthetic Approach To Obtain Meso-N-Substituted Porphyrins. *J. Org. Chem.* **2014**, *79* (14), 6424–6434. https://doi.org/10.1021/jo5005586.

(60) Fulmer, G. R.; Miller, A. J. M.; Sherden, N. H.; Gottlieb, H. E.; Nudelman, A.; Stoltz, B. M.; Bercaw, J. E.; Goldberg, K. I. NMR Chemical Shifts of Trace Impurities: Common Laboratory Solvents, Organics, and Gases in Deuterated Solvents Relevant to the Organometallic Chemist. *Organometallics* **2010**, *29* (9), 2176–2179. https://doi.org/10.1021/om100106e.

(61) Frisch, M. J.; Trucks, G. W.; Schlegel, H. B.; Scuseria, G. E.; Robb, M. A.; Cheeseman, J. R.; Scalmani, G.; Barone, V.; Petersson, G. A.; Nakatsuji, H.; Li, X.; Caricato, M.; Marenich, A. V.; Bloino, J.; Janesko, B. G.; Gomperts, R.; Mennucci, B.; Hratchian, H. P.; Ortiz, J. V.; Izmaylov, A. F.; Sonnenberg, J. L.; Williams-Young, D.; Ding, F.; Lipparini, F.; Egidi, F.; Goings, J.; Peng, B.; Petrone, A.; Henderson, T.; Ranasinghe, D.; Zakrzewski, V. G.; Gao, J.; Rega, N.; Zheng, G.; Liang, W.; Hada, M.; Ehara, M.; Toyota, K.; Fukuda, R.; Hasegawa, J.; Ishida, M.; Nakajima, T.; Honda, Y.; Kitao, O.; Nakai, H.; Vreven, T.; Throssell, K.; J. A. Montgomery, J.; Peralta, J. E.; Ogliaro, F.; Bearpark, M. J.; Heyd, J. J.; Brothers, E. N.; Kudin, K. N.; Staroverov, V. N.; Keith, T. A.; Kobayashi, R.; Normand, J.; Raghavachari, K.; Rendell, A. P.; Burant, J. C.; Iyengar, S. S.; Tomasi, J.; Cossi, M.; Millam, J. M.; Klene, M.; Adamo, C.; Cammi, R.; Ochterski, J. W.; Martin, R. L.; Morokuma, K.; Farkas, O.; Foresman, J. B.; Fox, D. J. *Gaussian 16, Revision C.01, Gaussian, Inc.: Wallingford CT*; 2016.

(62) Becke, A. D. Density-functional Thermochemistry. III. The Role of Exact Exchange. *J. Chem. Phys.* **1993**, *98* (7), 5648–5652. https://doi.org/10.1063/1.464913.

(63) Grimme, S.; Ehrlich, S.; Goerigk, L. Effect of the Damping Function in Dispersion Corrected Density Functional Theory. *J. Comput. Chem.* **2011**, *32* (7), 1456–1465. https://doi.org/10.1002/jcc.21759.

(64) *Chemcraft - Graphical Software for Visualization of Quantum Chemistry Computations. Https://Www.Chemcraftprog.Com.*

(65) Chai, J.-D.; Head-Gordon, M. Long-Range Corrected Hybrid Density Functionals with Damped Atom–Atom Dispersion Corrections. *Phys. Chem. Chem. Phys.* **2008**, *10* (44), 6615–6620. https://doi.org/10.1039/B810189B.

(66) Balaban, M. C.; Eichhofer, A.; Buth, G.; Hauschild, R.; Szmytkowski, J.; Kalt, H.; Balaban, T. S. Programmed Metalloporphyrins for Self-Assembly within Light-Harvesting Stacks: (5,15-Dicyano-10,20-Bis(3,5-Di-Tert-Butylphenyl)Porphyrinato)Zinc(II) and Its Push−Pull 15-N,N-Dialkylamino-5-Cyano Congeners Obtained by a Facile Direct Amination. *J. Phys. Chem. B* **2008**, *112* (17), 5512–5521. https://doi.org/10.1021/jp801510b.

(67) Balaban, M. C.; Chappaz-Gillot, C.; Canard, G.; Fuhr, O.; Roussel, C.; Balaban, T. S. Metal Catalyst-Free Amination of Meso-Bromoporphyrins: An Entry to Supramolecular Porphyrinoid Frameworks. *Tetrahedron* **2009**, *65*, 3733–3739.

(68) Yamashita, K.; Kataoka, K.; Asano, M. S.; Sugiura, K. Catalyst-Free Aromatic Nucleophilic Substitution of Meso-Bromoporphyrins with Azide Anion: Efficient Synthesis and Structural Analyses of Meso-Azidoporphyrins. *Org. Lett.* **2012**, *14* (1), 190–193. https://doi.org/10.1021/ol202973z.

(69) Yamashita, K.; Kataoka, K.; Takeuchi, S.; Sugiura, K. Metal-Free Synthesis of Meso-Aminoporphyrins through Reduction of Meso-Azidoporphyrins Generated in Situ by Nucleophilic Substitution Reactions of Meso-Bromoporphyrins. *J. Org. Chem.* **2016**, *81* (22), 11176–11184. https://doi.org/10.1021/acs.joc.6b02159.

(70) Kielmann, M.; Flanagan, K. J.; Norvaiša, K.; Intrieri, D.; Senge, M. O. Synthesis of a Family of Highly Substituted Porphyrin Thioethers via Nitro Displacement in 2,3,7,8,12,13,17,18-Octaethyl-5,10,15,20-Tetranitroporphyrin. *J. Org. Chem.* **2017**, *82* (10), 5122–5134. https://doi.org/10.1021/acs.joc.7b00328.

(71) Yamashita, K.; Kataoka, K.; Pham Qui Van, H.; Ogawa, T.; Sugiura, K. Versatile and Catalyst-Free Methods for the Introduction of Group-16 Elements at the Meso-Positions of

Diarylporphyrins. *Asian J. Org. Chem.* **2018**, *7* (12), 2468–2478. https://doi.org/10.1002/ajoc.201800538.

(72) Sample, H. C.; Senge, M. O. Nucleophilic Aromatic Substitution (SNAr) and Related Reactions of Porphyrinoids: Mechanistic and Regiochemical Aspects. *Eur. J. Org. Chem.* **2020**, *2021* (1), 7–42. https://doi.org/10.1002/ejoc.202001183.

(73) Yatskou, M. M.; Koehorst, R. B. M.; Donker, H.; Schaafsma, T. J. Spectroscopic Properties of a Self-Assembled Zinc Porphyrin Tetramer I. Steady State Optical Spectroscopy. *J. Phys. Chem. A* **2001**, *105* (51), 11425–11431. https://doi.org/10.1021/jp010410p.

(74) Yatskou, M. M.; Koehorst, R. B. M.; van Hoek, A.; Donker, H.; Schaafsma, T. J.; Gobets, B.; van Stokkum, I.; van Grondelle, R. Spectroscopic Properties of a Self-Assembled Zinc Porphyrin Tetramer II. Time-Resolved Fluorescence Spectroscopy. *J. Phys. Chem. A* **2001**, *105* (51), 11432–11440. https://doi.org/10.1021/jp010411h.

(75) Yatskou, M. M.; Donker, H.; Novikov, E. G.; Koehorst, R. B. M.; van Hoek, A.; Apanasovich, V. V.; Schaafsma, T. J. Nonisotropic Excitation Energy Transport in Organized Molecular Systems: Monte Carlo Simulation-Based Analysis of Fluorescence and Fluorescence Anisotropy Decay. *J. Phys. Chem. A* **2001**, *105* (41), 9498–9508. https://doi.org/10.1021/jp0044227.

(76) Funatsu, K.; Imamura, T.; Ichimura, A.; Sasaki, Y. Synthesis and Properties of Cyclic Ruthenium(II) Porphyrin Tetramers. *Inorg. Chem.* **1998**, *37* (8), 1798–1804. https://doi.org/10.1021/ic970884w.

(77) Jensen, R. A.; Kelley, R. F.; Joong Lee, S.; Wasielewski, M. R.; Hupp, J. T.; Tiede, D. M. Fast Energy Transfer within a Self-Assembled Cyclic Porphyrin Tetramer. *Chem. Commun.* **2008**, No. 16, 1886–1888. https://doi.org/10.1039/B718628B.

(78) Kelley, R. F.; Goldsmith, R. H.; Wasielewski, M. R. Ultrafast Energy Transfer within Cyclic Self-Assembled Chlorophyll Tetramers. *J. Am. Chem. Soc.* **2007**, *129* (20), 6384–6385. https://doi.org/10.1021/ja071362a.

(79) Shinozaki, Y.; Ohkubo, K.; Fukuzumi, S.; Sugawa, K.; Otsuki, J. Cyclic Tetramers of Zinc Chlorophylls as a Coupled Light-Harvesting Antenna–Charge-Separation System. *Chem. – Eur. J.* **2016**, *22* (3), 1165–1176. https://doi.org/10.1002/chem.201503789.

(80) Shinozaki, Y.; Tsubomura, T.; Sugawa, K.; Otsuki, J. Construction of Dendrimers with a Square-Shaped Core Consisting of Zinc Chlorophyll Assembly via Intermolecular Nitrogen–Zinc Coordination. *Tetrahedron Lett.* **2016**, *57* (1), 48–52. https://doi.org/10.1016/j.tetlet.2015.11.057.

(81) Kamada, T.; Aratani, N.; Ikeda, T.; Shibata, N.; Higuchi, Y.; Wakamiya, A.; Yamaguchi, S.; Kim, K. S.; Yoon, Z. S.; Kim, D.; Osuka, A. High Fidelity Self-Sorting Assembling of Meso-Cinchomeronimide Appended Meso-Meso Linked Zn(II) Diporphyrins. *J. Am. Chem. Soc.* **2006**, *128* (23), 7670–7678. https://doi.org/10.1021/ja0611137.

(82) Tsuda, A.; Nakamura, T.; Sakamoto, S.; Yamaguchi, K.; Osuka, A. A Self-Assembled Porphyrin Box from Meso–Meso-Linked Bis{5-p-Pyridyl-15-(3,5-Di-Octyloxyphenyl)Porphyrinato Zinc(II)}. *Angew. Chem., Int. Ed.* **2002**, *41* (15), 2817–2821. https://doi.org/10.1002/1521-3773(20020802)41:15<2817::AID-ANIE2817>3.0.CO;2-0.

(83) Shachter, A. M.; Fleischer, E. B.; Haltiwanger, R. C. Characterization of a 5-Pyridyl-10,15,20-Triphenylporphyrinatozinc(II) Polymer. *J. Chem. Soc., Chem. Commun.* **1988**, No. 14, 960–961. https://doi.org/10.1039/C39880000960.

(84) Shinozaki, Y.; Richards, G.; Ogawa, K.; Yamano, A.; Ohara, K.; Yamaguchi, K.; Kawano, S.; Tanaka, K.; Araki, Y.; Wada, T.; Otsuki, J. Double Helices of a Pyridine-Appended Zinc Chlorophyll Derivative. *J. Am. Chem. Soc.* **2013**, *135* (14), 5262–5265. https://doi.org/10.1021/ja400493e.

(85) P.S. Clezy; D.C. Craig; V.J. James; A.D. Rae; J.F. McConnell. DTCOPM : 10,10'-Dithio-Bis(Coproporphyrin II Tetramethyl Ester). *Crystal Structure Communications* **1979**, *8*, 605.

(86) Ryan, A. A.; Plunkett, S.; Casey, A.; McCabe, T.; Senge, M. O. From Thioether Substituted Porphyrins to Sulfur Linked Porphyrin Dimers: An Unusual SNAr via Thiolate Displacement? *Chem. Commun.* **2014**, *50* (3), 353–355. https://doi.org/10.1039/c3cc46828c.

(87) Jiang, P.; Zhao, T.; Rong, J.; Yin, B.; Rao, Y.; Zhou, M.; Xu, L.; Song, J. Multi-(Phenylthio)Porphyrinato Ni(II) Compounds: Synthesis, Structures and Properties. *Chin. Chem. Lett.* **2021**, *32* (8), 2562–2566. https://doi.org/10.1016/j.cclet.2021.02.022.

(88) Gunderson, V. L.; Wasielewski, M. R. Self-Assembly of a Chlorophyll-Based Cyclic Trimer: Structure and Intramolecular Energy Transfer. *Chem. Phys. Lett.* **2013**, *556*, 303–307. https://doi.org/10.1016/j.cplett.2012.12.025.

(89) Otsuki, J.; Okumura, T.; Sugawa, K.; Kawano, S.; Tanaka, K.; Hirao, T.; Haino, T.; Lee, Y. J.; Kang, S.; Kim, D. A Light-Harvesting/Charge-Separation Model with Energy Gradient

Made of Assemblies of Meta-Pyridyl Zinc Porphyrins. *Chem. − Eur. J.* **2021**, *27* (12), 4053–4063. https://doi.org/10.1002/chem.202003327.

(90) Macrae, C. F.; Sovago, I.; Cottrell, S. J.; Galek, P. T. A.; McCabe, P.; Pidcock, E.; Platings, M.; Shields, G. P.; Stevens, J. S.; Towler, M.; Wood, P. A. It Mercury 4.0: From Visualization to Analysis, Design and Prediction. *J. Appl. Cryst.* **2020**, *53* (1), 226–235. https://doi.org/10.1107/S1600576719014092.

(91) Kadish, K. M.; Caemelbecke, E. V.; Royal, G. Electrochemistry of Metalloporphyrins in Nonaqueous Media. In *The Porphyrin Handbook*; Kadish, Karl. M., Smith, K. M., Guilard, R., Eds.; Academic Press, 2000; Vol. 8, pp 1–114.

(92) Kurotobi, K.; Kim, K. S.; Noh, S. B.; Kim, D.; Osuka, A. A Quadruply Azulene-Fused Porphyrin with Intense Near-IR Absorption and a Large Two-Photon Absorption Cross Section. *Angew. Chem., Int. Ed.* **2006**, *45* (24), 3944–3947. https://doi.org/10.1002/anie.200600892.

(93) Gouterman, M. Study of the Effects of Substitution on the Absorption Spectra of Porphin. *J. Chem. Phys.* **1959**, *30* (5), 1139–1161. https://doi.org/10.1063/1.1730148.

(94) Gouterman, M. Spectra of Porphyrins. *J. Mol. Spectrosc.* **1961**, *6*, 138–163. https://doi.org/10.1016/0022-2852(61)90236-3.

(95) Devillers, C. H.; Fleurat-Lessard, P.; Lucas, D. “Porphine,” the Fully Unsubstituted Porphyrin: A Comprehensive Overview. In *Handbook of Porphyrin Science*; Kadish, K. M., Smith, K. M., Guilard, R., Eds.; World Scientific Publishing Company, 2016; Vol. 37, pp 75–231. https://doi.org/10.1142/9789813149571_0002.

(96) Gouterman, M. 1 - Optical Spectra and Electronic Structure of Porphyrins and Related Rings. In *The Porphyrins*; Dolphin, D., Ed.; Academic Press, 1978; pp 1–165. https://doi.org/10.1016/B978-0-12-220103-5.50008-8.

(97) Giraudeau, A.; Lobstein, S.; Ruhlmann, L.; Melamed, D.; Barkigia, K. M.; Fajer, J. Electrosynthesis, Electrochemistry, and Crystal Structure of the Tetracationic Zn-Meso-Tetrapyridiniumyl-β-Octaethylporphyrin. *J. Porphyrins Phthalocyanines* **2001**, *05* (11), 793–797. https://doi.org/10.1002/jpp.547.

(98) Renner Mark, W.; Bochot, C.; Héroux, A.; Mansuy, D.; Battioni, P. Structural, Electrochemical, and Spectroscopic Properties of a Class of Dodecasubstituted Iron Porphyrins Bearing Four Positive Charges Close to the Metal. *Eur. J. Org. Chem.* **2007**, *2007* (17), 2426–2433. https://doi.org/10.1002/ejic.200601181.

(99) Deisenhofer, J.; Michel, H. The Photosynthetic Reaction Center from the Purple Bacterium Rhodopseudomonas Viridis. *Science* **1989**, *245* (4925), 1463–1473. https://doi.org/10.1126/science.245.4925.1463.

(100) Jin, L.-M.; Chen, L.; Yin, J.-J.; Guo, C.-C.; Chen, Q.-Y. A Facile and Potent Synthesis of Meso-Meso-Linked Porphyrins Arrays Using Iodine(III) Reagents. *Eur. J. Org. Chem.* **2005**, *2005* (18), 3994–4001.

(101) Ouyang, Q.; Zhu, Y.-Z.; Zhang, C.-H.; Yan, K.-Q.; Li, Y.-C.; Zheng, J.-Y. An Efficient PIFA-Mediated Synthesis of Fused Diporphyrin and Triply-Singly Interlacedly Linked Porphyrin Array. *Org. Lett.* **2009**, *11* (22), 5266.

(102) Osuka, A.; Shimidzu, H. Meso, Meso-Linked Porphyrin Arrays. *Angew. Chem., Int. Ed.* **1997**, *36* (1-2), 135–137. https://doi.org/10.1002/anie.199701351.

(103) Ogawa, T.; Nishimoto, Y.; Ono, N.; Yoshida, N.; Osuka, A. One-Pot Electrochemical Formation of Meso,Meso-Linked Porphyrin Arrays. *Chem. Commun.* **1998**, No. 3, 337–338. https://doi.org/10.1039/a707653c.

(104) Ogawa, T.; Nishimoto, Y.; Yoshida, N.; Ono, N.; Osuka, A. Completely Regioselective Synthesis of Directly Linked Meso,Meso and Meso,β Porphyrin Dimers by One-Pot Electrochemical Oxidation of Metalloporphyrins. *Angew. Chem., Int. Ed. Engl.* **1999**, *38* (1–2), 176–179. https://doi.org/10.1002/(sici)1521-3773(19990115)38:1/2<176::aid-anie176>3.0.co;2-a.

(105) Shi, X.; Liebeskind, L. S. 3-Cyclobutenyl-1,2-Dione-Substituted Porphyrins. 2. A Simple and General Entry to Quinone-Porphyrin-Porphyrin-Quinone Tetrads and Related Molecules. *J. Org. Chem.* **2000**, *65* (6), 1665–1671.

(106) Diev, V. V.; Hanson, K.; Zimmerman, J. D.; Forrest, S. R.; Thompson, M. E. Fused Pyrene-Diporphyrins: Shifting Near-Infrared Absorption to 1.5 Mm and Beyond. *Angew. Chem., Int. Ed.* **2010**, *49* (32), 5523–5526. https://doi.org/10.1002/anie.201002669.

(107) Inokuma, Y.; Ono, N.; Uno, H.; Kim, D. Y.; Noh, S. B.; Kim, D.; A.Osuka. Enlarged P-Electronic Network of a Meso-Meso, b-b, b-b Triply Linked Dibenzoporphyrin Dimer That Exhibits a Large Two-Photon Absorption Cross Section. *Chem. Commun.* **2005**, 3782.

(108) Bonifazi, D.; Accorsi, G.; Armaroli, N.; Song, F.; Palkar, A.; Echegoyen, L.; Scholl, M.; Seiler, P.; Jaun, B.; Diederich, F. Oligoporphyrin Arrays Conjugated to [60]Fullerene: Preparation, NMR Analysis, and Photophysical and Electrochemical Properties. *Helv. Chim. Acta* **2005**, *88* (7), 1839–1884. https://doi.org/10.1002/hlca.200590144.

(109) Hiroto, S.; Osuka, A. Meso-Alkyl-Substituted Meso-Meso Linked Diporphyrins and Meso-Alkyl-Substituted Meso-Meso, β-β, β-β Triply Linked Diporphyrins. *J. Org. Chem.* **2005**, *70* (10), 4054–4058. https://doi.org/10.1021/jo0502192.

(110) Ikeda, T.; Lintuluoto, J. M.; Aratani, N.; Yoon, Z. S.; Kim, D.; Osuka, A. Synthesis of Doubly Strapped Meso-Meso-Linked Porphyrin Arrays and Triply Linked Conjugated Porphyrin Tapes. *Eur. J. Org. Chem.* **2006**, *2006* (14), 3193–3204. https://doi.org/10.1002/ejoc.200600289.

(111) Jun-i, Y.; Fukui, N.; Furukawa, K.; Osuka, A. Metalation Control of Open-Shell Character in Meso-Meso Linked Porphyrin Meso-Oxy Radical Dimers. *Chem. − Eur. J.* **2018**, *24* (7), 1528–1532. https://doi.org/10.1002/chem.201705769.

(112) Wu, C.-A.; Chiu, C.-L.; Mai, C.-L.; Lin, Y.-S.; Yeh, C.-Y. A Waterwheel-Shaped Meso–Meso-Linked Porphyrin Pentamer. *Chem. − Eur. J.* **2009**, *15* (18), 4534–4537. https://doi.org/10.1002/chem.200900378.

(113) Tsuda, A.; Furuta, H.; Osuka, A. Syntheses, Structural Characterizations, and Optical and Electrochemical Properties of Directly Fused Diporphyrins. *J. Am. Chem. Soc.* **2001**, *123* (42), 10304–10321. https://doi.org/10.1021/ja0110933.

FOR TABLE OF CONTENTS ONLY

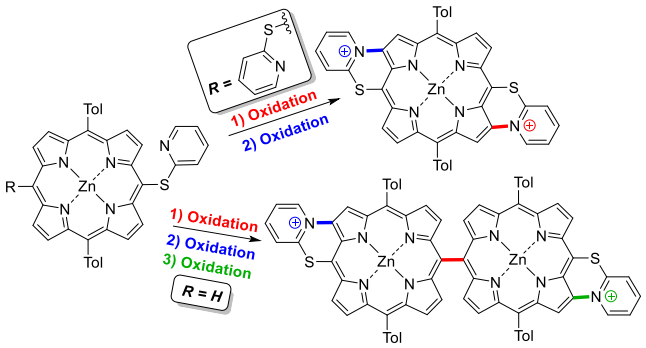

SYNOPSIS. The (electro)chemical oxidation of original zinc(II) *meso*-(pyridin-2-ylthio)porphyrins affords the C-N fused (bis)pyridinium derivatives in a stepwise manner. When one *meso* position remains free, the first oxidative reaction consists in the *meso*,*meso* C-C dimerization. The resulting pyridinium derivatives exhibits important changes in their physico-chemical properties and the X-ray crystallographic structures of two C-N fused monomers are presented.